Condensed Matter Physics 2009, Vol. 12, No 2, pp. 275–294

CONDENSED MATTER PHYSICS

Longitudinal relaxation of $ND_4D_2PO_4$ type antiferroelectrics. Piezoelectric resonance and sound attenuation

R.R.Levitskii[1], I.R.Zachek[2], A.P.Moina[1], A.S.Vdovych[1]

[1] Institute for Condensed Matter Physics of the National Academy of Sciences of Ukraine, 1 Svientsitskii str, 79011 Lviv, Ukraine

[2] Lviv Polytechnic National University, 12 Bandera Str., 79013 Lviv, Ukraine

Received April 2, 2009, in final form May 18, 2009

Within the framework of the modified proton model with taking into account the interaction with the shear strain ε_6, a dynamic dielectric response of $ND_4D_2PO_4$ type antiferroelectrics is considered. Dynamics of the piezoelectric strain is taken into account. Experimentally observed phenomena of crystal clamping by high frequency electric field, piezoelectric resonance and microwave dispersion are described. Ultrasound velocity and attenuation are calculated. Character of behaviour of attenuation in the paraelectric phase and the existence of a cut-off frequency in the frequency dependence of attenuation are predicted. At the proper choice of the parameters, a good quantitative description of experimental data for longitudinal static dielectric, piezoelectric and elastic characteristics and sound velocity for $ND_4D_2PO_4$ and $NH_4H_2PO_4$ is obtained in the paraelectric phase.

Key words: *antiferroelectrics, dielectric permittivity, piezoelectric resonance*

PACS: *77.22.Ch, 77.22.Gm, 77.65.Bn 77.84.Fa, 77.65.Fs*

1. Introduction

Ferroelectric compounds of the MD_2XO_4 (M=K, D_4; x=P, As) type crystallize in the $\bar{4}\cdot m$ class of the tetragonal syngony (space group $I\bar{4}2d$ with non-centrosymmetric point group D_{2d}) in the paraelectric phase and possess piezoelectric properties. When appropriate electric fields and shear stresses are applied, one can explore the role of piezoelectric coupling in the phase transition and in the formation of physical characteristics of the crystals. Theoretical investigations of the role of piezoelectricity in the KH_2PO_4 type ferroelectricity were initiated in [1], where the Slater theory [2] was modified by taking into account the splitting of the lowest ferroelectric energy level of the proton subsystem due to the strain ε_6.

Important results for strained ferroelectric compounds of the KH_2PO_4 type were obtained in [3–11]. In [3,4] the proton ordering model was modified by taking into account the ε_6 contributions to the proton subsystem energy linear in strain. The obtained Hamiltonian contains a deformational molecular field and takes splitting of lateral proton configurations into account. Later [5–7] all possible splittings of proton configuration energies by the strain ε_6 were taken into account. In [5] a phase transition in the strained $K(H_{0,12}D_{0,88})_2PO_4$ crystal was explored; its thermodynamic, longitudinal dielectric, piezoelectric, and elastic characteristics were calculated; the effect of the stress σ_6 on the calculated quantities was studied. Similar calculations of thermodynamic, longitudinal and transverse dielectric, piezoelectric, and elastic characteristics of KH_2PO_4 type ferroelectrics were performed in [6–8] with tunneling taken into account. A good description of experimental data for the KH_2PO_4 ferroelectrics and $NH_4H_2PO_4$ antiferroelectrics in the paraelectric phase was obtained. In [9–11], the effect of longitudinal electric field on the physical characteristics of $K(H_{0,12}D_{0,88})_2PO_4$ and KH_2PO_4 was studied; a satisfactory quantitative agreement with the available experimental data was obtained.

© R.R.Levitskii, I.R.Zachek, A.P.Moina, A.S.Vdovych

We should also mention the paper [12], where the mechanism of spontaneous strain ε_6 formation in the KH_2PO_4 type ferroelectrics and the role of proton interactions with acoustic lattice vibrations in this process were explored.

In [5–11], the dynamic properties of KH_2PO_4 type ferroelectrics were not studied with taking into account the piezoelectric coupling. Such a problem, however, is very important. Due to the effect of tunneling suppression in KH_2PO_4 family crystals found in [13–15], and due to the principal difficulties arising at calculations of dynamic characteristics in the presence of tunneling, this problem should be approached by neglecting tunneling. In [16–19], within the framework of the modified proton ordering models, the thermal, longitudinal and transverse dielectric, piezoelectric, and elastic characteristics of the KH_2PO_4 family ferroelectrics were calculated. The relaxational phenomena in these crystals were explored; sound velocity and attenuation were obtained. It was shown that for a proper choice of the theory parameters, the experimental data for longitudinal dynamic characteristics of these crystals should be taken into account.

Description of dynamic dielectric characteristics of the $ND_4D_2PO_4$ type antiferroelectrics [20–22] was restricted to the static limit and high-frequency relaxation. The attempts to explore the piezoelectric resonance within a model that does not take into account the piezoelectric coupling are pointless. The traditional proton ordering model for the $ND_4D_2PO_4$ type antiferroelectrics does not allow one to describe the difference of the behaivor of free and clamped crystals in the static limit or the effect of crystal clamping produced by high-frequency field. It seems natural to calculate the dynamic characteristics of the $ND_4D_2PO_4$ type antiferroelectrics using the proton ordering model proposed in [5,6,18] in a wide frequency range from 10^3 kHz up to 10^{12} Hz, including the piezoelectric resonance region as well.

In the present paper, following the approach developed in [23,24], within the framework of the modified proton ordering model with taking into account the coupling with shear strain ε_6, we calculate the longitudinal dynamic dielectric, piezoelectric, and elastic characteristics of the $ND_4D_2PO_4$ type antiferroelectrics and explore their temperature and frequency dependences. The effect of crystal clamping produced by a high-frequency longitudinal electric field is studied. Sound velocity and attenuation in these crystals are also calculated.

2. Hamiltonian of proton ordering model

We shall consider a system of deuterons moving on the O–D...O bonds in deuterated $ND_4D_2PO_4$ type crystals. The primitive cell of the Bravais lattice of these crystals consists of two neighboring tetrahedra PO_4 along with four hydrogen bonds attached to one of them (the "A" type tetrahedron). The hydrogen bonds attached to the other tetrahedron ("B" type) belong to the four structural elements surrounding it. Spontaneous polarization in these crystals is zero due to antipolar ordering of dipole moments of hydrogen bonds. External fields applied along a, b, and c axes induce non-zero net polarization.

The model Hamiltonian, with taking into account the short-range and long-range interactions, in the presence of mechanical stress $\sigma_6 = \sigma_{xy}$ and external electric field E_3 directed along the crystallographic axis c, consists of the "seed" and pseudospin parts. The "seed" energy of a primitive cell corresponds to the lattice of heavy ions and is explicitly independent of the configurations of hydrogen bonds. The pseudospin part of the Hamiltonian includes long-range ($\hat{H}_{\rm long}$) and short-range ($\hat{H}_{\rm short}$) deuteron interactions as well as the effective interactions of deuterons with the electric field E_3. Hence,

$$\hat{H} = NU_{\rm seed} + \hat{H}_{\rm long} + \hat{H}_{\rm short} - \sum_{qf} \mu_{f3} E_3 \frac{\sigma_{qf}}{2}, \tag{2.1}$$

where N is the number of primitive cells; σ_{qf} is the operator of the z-component of a pseudospin describing the state of a deuteron in the q-th cell on the f-th bond. Eigenvalues of the operator $\sigma_{qf} = \pm 1$ correspond to the two possible equilibrium positions of the deuteron on the bond. Symmetry of the effective dipole moments of the primitive cells along the c-axis per one hydrogen

bond is as follows:

$$\mu_3 = \mu_{13} = \mu_{23} = \mu_{33} = \mu_{43}\,.$$

The "seed" energy $U_{\rm seed}$ is expressed in terms of the electric field E_3 and strain ε_6. It consists of the elastic, piezoelectric, and dielectric parts

$$U_{\rm seed} = \bar{v}\left(\frac{1}{2}c_{66}^{E0}\varepsilon_6^2 - e_{36}^0\varepsilon_6 E_3 - \frac{1}{2}\chi_{33}^{\varepsilon 0}E_3^2\right), \tag{2.2}$$

where $\bar{v} = \frac{v}{k_{\rm B}}$, v is the primitive cell volume; $k_{\rm B}$ is the Boltzmann constant; c_{66}^{E0}, e_{36}^0, $\chi_{33}^{\varepsilon 0}$ are the "seed" elastic constant, coefficient of piezoelectric stress, and dielectric susceptibility, respectively. The "seed" quantities determine the temperature behavior of the corresponding characteristics at temperatures far from the transition point $T_{\rm N}$.

The Hamiltonian $\hat{H}_{\rm long}$ includes the long-range interactions between deuterons and an indirect lattice-mediated deuteron interactions taken into account within the mean field approximation, as well as the linear in the strain ε_6 molecular field [3,4], induced by piezoelectric coupling

$$\hat{H}_{\rm long} = \frac{1}{2}\sum_{\substack{qq'\\ ff'}} J_{ff'}(qq')\frac{\langle\sigma_{qf}\rangle}{2}\frac{\langle\sigma_{q'f'}\rangle}{2} - \sum_{qf} 2\mu F_{qf}\frac{\sigma_{qf}}{2}\,. \tag{2.3}$$

Here

$$\begin{aligned} 2\mu F_{q_3^1} &= \mp 2\nu_a(\mathbf{k}^z)\eta^{(1)}\mathrm{e}^{\mathrm{i}\mathbf{k}^z\mathbf{a}_q} + 2\nu_c(0)\eta^{(1)z} - 2\psi_6\varepsilon_6,\\ 2\mu F_{q_4^2} &= \pm 2\nu_a(\mathbf{k}^z)\eta^{(1)}\mathrm{e}^{\mathrm{i}\mathbf{k}^z\mathbf{a}_q} + 2\nu_c(0)\eta^{(1)z} - 2\psi_6\varepsilon_6, \end{aligned} \tag{2.4}$$

and we took into account the fact that the single-particle deuteron distribution functions can be presented as a sum of a modulated part and uniform terms induced by the longitudinal electric field

$$\langle\sigma_{q_3^1}\rangle = \mp\eta^{(1)}\mathrm{e}^{\mathrm{i}\mathbf{k}^z\mathbf{a}_q} + \eta^{(1)z},\ \langle\sigma_{q_4^2}\rangle = \pm\eta^{(1)}\mathrm{e}^{\mathrm{i}\mathbf{k}^z\mathbf{a}_q} + \eta^{(1)z}\,.$$

In (2.4) we use the following notations

$$4\nu_a(\mathbf{k}^z) = J_{11}(\mathbf{k}^z) - J_{13}(\mathbf{k}^z), \qquad 4\nu_c(0) = J_{11}(0) + 2J_{12}(0) + J_{13}(0),$$
$$J_{ff'}(\mathbf{k}^z) = \sum_{\mathbf{a}_q - \mathbf{a}_{q'}} J_{ff'}(qq')\mathrm{e}^{-\mathrm{i}\mathbf{k}^z(\mathbf{a}_q - \mathbf{a}_{q'})};$$

$\mathbf{k}^z = 1/2(\mathbf{b}_1 + \mathbf{b}_2 + \mathbf{b}_3)$, $\mathbf{b}_1$, $\mathbf{b}_2$, $\mathbf{b}_3$ are vectors of the reciprocal lattice; $\mathrm{e}^{\mathrm{i}\mathbf{k}^z\mathbf{a}_q} = \pm 1$, ψ_6 is the deformational potential.

The Hamiltonian $\hat{H}_{\rm short}$ reads [18]:

$$\begin{aligned} \hat{H}_{\rm short} \;=\; & \sum_q \left\{ \left(-\frac{\delta_{s6}}{4} + \frac{\delta_{16}}{2}\right)\varepsilon_6\left(\frac{\sigma_{q1}}{2} + \frac{\sigma_{q2}}{2} + \frac{\sigma_{q3}}{2} + \frac{\sigma_{q4}}{2}\right)\right.\\ & + (-\delta_{s6} - 2\delta_{16})\,\varepsilon_6\left(\frac{\sigma_{q1}}{2}\frac{\sigma_{q2}}{2}\frac{\sigma_{q3}}{2} + \frac{\sigma_{q1}}{2}\frac{\sigma_{q2}}{2}\frac{\sigma_{q4}}{2} + \frac{\sigma_{q1}}{2}\frac{\sigma_{q3}}{2}\frac{\sigma_{q4}}{2} + \frac{\sigma_{q2}}{2}\frac{\sigma_{q3}}{2}\frac{\sigma_{q4}}{2}\right)\\ & + (V_a + \delta_{a6}\varepsilon_6)\left(\frac{\sigma_{q1}}{2}\frac{\sigma_{q2}}{2} + \frac{\sigma_{q3}}{2}\frac{\sigma_{q4}}{2}\right) + (V_a - \delta_{a6}\varepsilon_6)\left(\frac{\sigma_{q2}}{2}\frac{\sigma_{q3}}{2} + \frac{\sigma_{q4}}{2}\frac{\sigma_{q1}}{2}\right)\\ & \left. + U_a\left(\frac{\sigma_{q1}}{2}\frac{\sigma_{q3}}{2} + \frac{\sigma_{q2}}{2}\frac{\sigma_{q4}}{2}\right) + \Phi_a\frac{\sigma_{q1}}{2}\frac{\sigma_{q2}}{2}\frac{\sigma_{q3}}{2}\frac{\sigma_{q4}}{2}\right\}, \end{aligned} \tag{2.5}$$

where we use the notations

$$V_a = \frac{1}{2}\varepsilon' - \frac{1}{2}w_1', \qquad U_a = \frac{1}{2}\varepsilon' + \frac{1}{2}w_1', \qquad \Phi_a = 2\varepsilon' - 8w' + 2w_1'.$$

Here

$$\varepsilon' = \varepsilon_s - \varepsilon_a; \quad w' = \varepsilon_1 - \varepsilon_a; \quad w_1' = \varepsilon_0 - \varepsilon_a\,,$$

where ε_s, ε_a, ε_1, ε_0 are the configurational energies of deuterons, and ε', w', w_1' are the antiferroelectric energies of the extended Slater-Takagi model.

Considering the peculiarities of the crystal structure of $ND_4D_2PO_4$ type crystals, we shall use the four-particle cluster approximation [25]. The longitudinal static dielectric and elastic characteristics can be calculated using the thermodynamic potential, which in the cluster approximation reads [18]:

$$G = NU_{\rm seed} + \frac{1}{2}\sum_{\substack{qq'\\ ff'}} J_{ff'}(qq')\frac{\langle\sigma_{qf}\rangle}{2}\frac{\langle\sigma_{q'f'}\rangle}{2} - \frac{1}{2}T\sum_q\sum_{f=1}^{4}\ln Z_{q1f} - T\sum_q \ln Z_{q4} - N\bar{v}\sigma_6\varepsilon_6\,, \quad (2.6)$$

where $Z_{q1f} = {\rm Sp}\,{\rm e}^{-\beta\hat{H}^{(1)}_{qf}}$, $Z_{q4} = {\rm Sp}\,{\rm e}^{-\beta\hat{H}^{(4)}_{q}}$ are the single-particle and four-particle partition functions. The single-particle $\hat{H}^{(1)}_{qf}$ and four-particle $\hat{H}^{(4)}_{q}$ deuteron Hamiltonians read

$$\hat{H}^{(1)}_{q_3^1} = \mp\frac{1}{\beta}\bar{x}_q\frac{\sigma_{q_3^1}}{2} + \frac{1}{\beta}\bar{z}\frac{\sigma_{q_3^1}}{2}, \qquad \hat{H}^{(1)}_{q_4^2} = \pm\frac{1}{\beta}\bar{x}_q\frac{\sigma_{q_4^2}}{2} + \frac{1}{\beta}\bar{z}\frac{\sigma_{q_4^2}}{2}\,, \quad (2.7)$$

$$\begin{aligned}\hat{H}^{(4)}_{q} = {} & \left(-\frac{\delta_{s6}}{4} + \frac{\delta_{16}}{2}\right)\varepsilon_6\left(\frac{\sigma_{q1}}{2} + \frac{\sigma_{q2}}{2} + \frac{\sigma_{q3}}{2} + \frac{\sigma_{q4}}{2}\right)\\ & + (-\delta_{s6} - 2\delta_{16})\,\varepsilon_6\left(\frac{\sigma_{q1}}{2}\frac{\sigma_{q2}}{2}\frac{\sigma_{q3}}{2} + \frac{\sigma_{q1}}{2}\frac{\sigma_{q2}}{2}\frac{\sigma_{q4}}{2} + \frac{\sigma_{q1}}{2}\frac{\sigma_{q3}}{2}\frac{\sigma_{q4}}{2} + \frac{\sigma_{q2}}{2}\frac{\sigma_{q3}}{2}\frac{\sigma_{q4}}{2}\right)\\ & + (V_a + \delta_{a6}\varepsilon_6)\left(\frac{\sigma_{q1}}{2}\frac{\sigma_{q2}}{2} + \frac{\sigma_{q3}}{2}\frac{\sigma_{q4}}{2}\right) + (V_a - \delta_{a6}\varepsilon_6)\left(\frac{\sigma_{q2}}{2}\frac{\sigma_{q3}}{2} + \frac{\sigma_{q4}}{2}\frac{\sigma_{q1}}{2}\right)\\ & + U_a\left(\frac{\sigma_{q1}}{2}\frac{\sigma_{q3}}{2} + \frac{\sigma_{q2}}{2}\frac{\sigma_{q4}}{2}\right) + \Phi_a\frac{\sigma_{q1}}{2}\frac{\sigma_{q2}}{2}\frac{\sigma_{q3}}{2}\frac{\sigma_{q4}}{2}\\ & - \frac{1}{\beta}x_q\left(-\frac{\sigma_{q1}}{2} + \frac{\sigma_{q2}}{2} + \frac{\sigma_{q3}}{2} - \frac{\sigma_{q4}}{2}\right) - \frac{1}{\beta}z\left(\frac{\sigma_{q1}}{2} + \frac{\sigma_{q2}}{2} + \frac{\sigma_{q3}}{2} + \frac{\sigma_{q4}}{2}\right). \end{aligned} \quad (2.8)$$

Here we use the notations

$$\begin{aligned} x_q &= \beta(-\Delta_a{\rm e}^{{\rm i}\mathbf{k}^z\mathbf{a}_q} + 2\nu_a(\mathbf{k}^z)\eta^{(1)}{\rm e}^{{\rm i}\mathbf{k}^z\mathbf{a}_q}), \quad z = \beta(-\Delta_c + 2\nu_c(0)\eta^{(1)z} - 2\psi_6\varepsilon_6 + \mu_3E_3),\\ \bar{x}_q &= -\beta\Delta_a{\rm e}^{{\rm i}\mathbf{k}^z\mathbf{a}_q} + x_q, \qquad\qquad \bar{z} = -\beta\Delta_c + z, \end{aligned}$$

and Δ_a, Δ_c are the effective fields exerted by the neighboring hydrogen bonds O–D...O from outside the cluster.

Having calculated the eigenvalues of the single-particle and four-particle Hamiltonians, we present the thermodynamic potential per unit cell in the form [18]:

$$\begin{aligned} g = {} & \frac{\bar{v}}{2}c_{66}^{E0}\varepsilon_6^2 - \bar{v}e_{36}^0\varepsilon_6E_3 + \frac{\bar{v}}{2}\chi_{33}^{\varepsilon 0}E_3^2 + 2T\ln 22\tilde{w}' + \tilde{\varepsilon}' + 2\nu_a(\mathbf{k}^z)\eta^{(1)2} + 2\nu_c(0)(\eta^{(1)z})^2\\ & - T\ln[1 - (\eta^{(1)} - \eta^{(1)z})^2] - T\ln[1 - (\eta^{(1)} + \eta^{(1)z})^2] - 2T\ln D_6 - \bar{v}\sigma_6\varepsilon_6. \end{aligned} \quad (2.9)$$

Here and further we note $\tilde{\varepsilon}' = \frac{\varepsilon'}{k_{\rm B}}$, $\tilde{w}' = \frac{w'}{k_{\rm B}}$.

From the conditions of thermodynamic equilibrium

$$\frac{1}{\bar{v}}\left(\frac{\partial g}{\partial\varepsilon_6}\right)_{E_3} = 0, \quad \frac{1}{v}\left(\frac{\partial g}{\partial E_3}\right)_{\sigma_6} = -P_3 \quad (2.10)$$

we obtain (in the limit $w_1' \to \infty$) an equation for the strain ε_6 and polarization P_3:

$$\begin{aligned} \sigma_6 &= c_{66}^{E0}\varepsilon_6 - e_{36}^0E_3 - \frac{2}{v}\delta_{s6}\frac{N_{s6}}{D_6} + \frac{2}{v}\delta_{16}\frac{N_{16}{\rm ch}x}{D_6} + \frac{2}{\bar{v}}\delta_{a6}\frac{N_{a6}}{D_6} + \frac{4}{v}\psi_6\eta^{(1)z},\\ P_3 &= e_{36}^0\varepsilon_6 + \chi_{33}^{\varepsilon 0}E_3 + 2\frac{\mu_3}{v}\eta^{(1)z}. \end{aligned} \quad (2.11)$$

Here we use the notations

$$\begin{aligned}
N_s &= a\mathrm{ch}(2z+\beta\delta_{s6}\varepsilon_6), \qquad N_1 = b\mathrm{ch}(z-\beta\delta_{16}\varepsilon_6),\\
N_{s6} &= a\mathrm{sh}(2z+\beta\delta_{s6}\varepsilon_6), \qquad N_{16} = 4b\mathrm{sh}(z-\beta\delta_{16}\varepsilon_6), \qquad N_{a6} = a_6 - \frac{\mathrm{ch}2x}{a_6},\\
D_6 &= a\mathrm{ch}(2z+\beta\delta_{s6}\varepsilon_6) + \frac{1}{a_6}\mathrm{ch}2x + a_6 + d\\
&\quad + 2b[\mathrm{ch}(x+z-\beta\delta_{16}\varepsilon_6) + \mathrm{ch}(x-z+\beta\delta_{16}\varepsilon_6)],\\
a &= \mathrm{e}^{-\beta\varepsilon'}, \qquad b = \mathrm{e}^{-\beta w'}, \qquad d = \mathrm{e}^{-\beta w_1'}, \qquad a_6 = \mathrm{e}^{-\beta\delta_{a6}\varepsilon_6}.
\end{aligned}$$

3. Longitudinal dynamic permittivity of $ND_4D_2PO_4$ type crystals

The dynamic characteristics of the $ND_4D_2PO_4$ type crystals will be explored within the framework of the dynamic model of these crystals based on the stochastic Glauber approach [26], where the time dependence of the deuteron distribution functions is described by the following equation

$$-\alpha\frac{\mathrm{d}}{\mathrm{d}t}\left\langle\prod_f \sigma_{qf}\right\rangle = \sum_{f'}\left\langle\prod_f \sigma_{qf}\left[1-\sigma_{qf'}\tanh\frac{\beta}{2}\varepsilon^z_{qf}\right]\right\rangle, \tag{3.1}$$

where α is the time constant that effectively determines the time scale of the dynamic processes in the system; ε^z_{qf} is the local field acting on the f-th bond in the q-th cell in the presence of the field E_3. The fields can be determined from the Hamiltonian (2.8)

$$\begin{aligned}
\tanh\frac{\beta}{2}\varepsilon^z_{q1} &= \tanh\left\{-\frac{\beta}{4}(V_a+\delta_{a6}\varepsilon_6)\sigma_{q2} - \frac{\beta}{4}(V_a-\delta_{a6}\varepsilon_6)\sigma_{q4} - \frac{\beta}{4}U_a\sigma_{q3} - \frac{\beta}{16}\Phi_a\sigma_{q2}\sigma_{q3}\sigma_{q4}\right.\\
&\quad \left.-\frac{\beta}{4}\left(-\frac{\delta_{s6}\varepsilon_6}{2}-\delta_{16}\varepsilon_6\right)(\sigma_{q2}\sigma_{q3}+\sigma_{q3}\sigma_{q4}+\sigma_{q2}\sigma_{q4}) - \frac{\beta}{4}\left(-\frac{\delta_{s6}\varepsilon_6}{2}+\delta_{16}\varepsilon_6\right) - \frac{1}{2}z_{q14}\right\},\\
\tanh\frac{\beta}{2}\varepsilon^z_{q2} &= \tanh\left\{-\frac{\beta}{4}(V_a+\delta_{a6}\varepsilon_6)\sigma_{q1} - \frac{\beta}{4}(V_a-\delta_{a6}\varepsilon_6)\sigma_{q3} - \frac{\beta}{4}U_a\sigma_{q4} - \frac{\beta}{16}\Phi_a\sigma_{q1}\sigma_{q3}\sigma_{q4}\right.\\
&\quad \left.-\frac{\beta}{4}\left(-\frac{\delta_{s6}\varepsilon_6}{2}-\delta_{16}\varepsilon_6\right)(\sigma_{q1}\sigma_{q4}+\sigma_{q3}\sigma_{q4}+\sigma_{q1}\sigma_{q3}) - \frac{\beta}{4}\left(-\frac{\delta_{s6}\varepsilon_6}{2}+\delta_{16}\varepsilon_6\right) + \frac{1}{2}z_{q23}\right\},\\
\tanh\frac{\beta}{2}\varepsilon^z_{q3} &= \tanh\left\{-\frac{\beta}{4}(V_a+\delta_{a6}\varepsilon_6)\sigma_{q4} - \frac{\beta}{4}(V_a-\delta_{a6}\varepsilon_6)\sigma_{q2} - \frac{\beta}{4}U_a\sigma_{q1} - \frac{\beta}{16}\Phi_a\sigma_{q1}\sigma_{q2}\sigma_{q4}\right.\\
&\quad \left.-\frac{\beta}{4}\left(-\frac{\delta_{s6}\varepsilon_6}{2}-\delta_{16}\varepsilon_6\right)(\sigma_{q1}\sigma_{q2}+\sigma_{q1}\sigma_{q4}+\sigma_{q2}\sigma_{q4}) - \frac{\beta}{4}\left(-\frac{\delta_{s6}\varepsilon_6}{2}+\delta_{16}\varepsilon_6\right) + \frac{1}{2}z_{q23}\right\},\\
\tanh\frac{\beta}{2}\varepsilon^z_{q4} &= \tanh\left\{-\frac{\beta}{4}(V_a+\delta_{a6}\varepsilon_6)\sigma_{q3} - \frac{\beta}{4}(V_a-\delta_{a6}\varepsilon_6)\sigma_{q1} - \frac{\beta}{4}U_a\sigma_{q2} - \frac{\beta}{16}\Phi_a\sigma_{q1}\sigma_{q2}\sigma_{q4}\right.\\
&\quad \left.-\frac{\beta}{4}\left(-\frac{\delta_{s6}\varepsilon_6}{2}-\delta_{16}\varepsilon_6\right)(\sigma_{q1}\sigma_{q2}+\sigma_{q2}\sigma_{q3}+\sigma_{q1}\sigma_{q3}) - \frac{\beta}{4}\left(-\frac{\delta_{s6}\varepsilon_6}{2}+\delta_{16}\varepsilon_6\right) - \frac{1}{2}z_{q14}\right\},
\end{aligned} \tag{3.2}$$

where

$$z_{q14} = -x_q + z, \qquad z_{q23} = x_q + z.$$

The right hand sides in (3.2) can be written as

$$\begin{aligned}
\tanh\frac{\beta}{2}\varepsilon^z_{q1} &= P^z_{q14}\sigma_{q3} + Q^z_{q141}\sigma_{q2} + Q^z_{q142}\sigma_{q4} + R^z_{q14}\sigma_{q2}\sigma_{q3}\sigma_{q4}\\
&\quad + M^z_{q141}\sigma_{q2}\sigma_{q3} + M^z_{q142}\sigma_{q3}\sigma_{q4} + N^z_{q14}\sigma_{q2}\sigma_{q4} + L^z_{q14},\\
&\quad \dots\\
\tanh\frac{\beta}{2}\varepsilon^z_{q4} &= P^z_{q14}\sigma_{q2} + Q^z_{q241}\sigma_{q3} + Q^z_{q142}\sigma_{q1} + R^z_{q14}\sigma_{q1}\sigma_{q2}\sigma_{q4}\\
&\quad + M^z_{q141}\sigma_{q2}\sigma_{q3} + M^z_{q142}\sigma_{q1}\sigma_{q2} + N^z_{q14}\sigma_{q1}\sigma_{q3} + L^z_{q14}.
\end{aligned} \tag{3.3}$$

Equating the right hand sides of (3.2) and (3.3) and taking into account the fact that $\sigma_{qf} = \pm 1$, we find

$$\begin{aligned}
P^z_{q\,{}^{14}_{23}} &= \frac{1}{8}\Big(l^z_{q1\,{}^{14}_{23}} - l^z_{q2\,{}^{14}_{23}} + n^z_{q1\,{}^{14}_{23}} - n^z_{q2\,{}^{14}_{23}} + m^z_{q1\,{}^{14}_{23}} - m^z_{q2\,{}^{14}_{23}} + m^z_{q3\,{}^{14}_{23}} - m^z_{q4\,{}^{14}_{23}}\Big),\\
Q^z_{q\,{}^{14}_{23}1} &= \frac{1}{8}\Big(l^z_{q1\,{}^{14}_{23}} - l^z_{q2\,{}^{14}_{23}} - n^z_{q1\,{}^{14}_{23}} + n^z_{q2\,{}^{14}_{23}} + m^z_{q1\,{}^{14}_{23}} + m^z_{q2\,{}^{14}_{23}} - m^z_{q3\,{}^{14}_{23}} - m^z_{q4\,{}^{14}_{23}}\Big),\\
Q^z_{q\,{}^{14}_{23}2} &= \frac{1}{8}\Big(l^z_{q1\,{}^{14}_{23}} - l^z_{q2\,{}^{14}_{23}} - n^z_{q1\,{}^{14}_{23}} + n^z_{q2\,{}^{14}_{23}} - m^z_{q1\,{}^{14}_{23}} - m^z_{q2\,{}^{14}_{23}} + m^z_{q3\,{}^{14}_{23}} + m^z_{q4\,{}^{14}_{23}}\Big),\\
R^z_{q\,{}^{14}_{23}} &= \frac{1}{8}\Big(l^z_{q1\,{}^{14}_{23}} - l^z_{q2\,{}^{14}_{23}} + n^z_{q1\,{}^{14}_{23}} + n^z_{q2\,{}^{14}_{23}} - m^z_{q1\,{}^{14}_{23}} + m^z_{q2\,{}^{14}_{23}} - m^z_{q3\,{}^{14}_{23}} + m^z_{q4\,{}^{14}_{23}}\Big),\\
M^z_{q\,{}^{14}_{23}1} &= \frac{1}{8}\Big(l^z_{q1\,{}^{14}_{23}} + l^z_{q2\,{}^{14}_{23}} - n^z_{q1\,{}^{14}_{23}} - n^z_{q2\,{}^{14}_{23}} + m^z_{q1\,{}^{14}_{23}} - m^z_{q2\,{}^{14}_{23}} - m^z_{q3\,{}^{14}_{23}} + m^z_{q4\,{}^{14}_{23}}\Big),\\
M^z_{q\,{}^{14}_{23}2} &= \frac{1}{8}\Big(l^z_{q1\,{}^{14}_{23}} + l^z_{q2\,{}^{14}_{23}} - n^z_{q1\,{}^{14}_{23}} - n^z_{q2\,{}^{14}_{23}} - m^z_{q1\,{}^{14}_{23}} + m^z_{q2\,{}^{14}_{23}} + m^z_{q3\,{}^{14}_{23}} - m^z_{q4\,{}^{14}_{23}}\Big),\\
N^z_{q\,{}^{14}_{23}} &= \frac{1}{8}\Big(l^z_{q1\,{}^{14}_{23}} + l^z_{q2\,{}^{14}_{23}} + n^z_{q1\,{}^{14}_{23}} + n^z_{q2\,{}^{14}_{23}} - m^z_{q1\,{}^{14}_{23}} - m^z_{q2\,{}^{14}_{23}} - m^z_{q3\,{}^{14}_{23}} - m^z_{q4\,{}^{14}_{23}}\Big),\\
L^z_{q\,{}^{14}_{23}} &= \frac{1}{8}\Big(l^z_{q1\,{}^{14}_{23}} + l^z_{q2\,{}^{14}_{23}} + n^z_{q1\,{}^{14}_{23}} + n^z_{q2\,{}^{14}_{23}} + m^z_{q1\,{}^{14}_{23}} + m^z_{q2\,{}^{14}_{23}} + m^z_{q3\,{}^{14}_{23}} + m^z_{q4\,{}^{14}_{23}}\Big), \qquad (3.4)
\end{aligned}$$

where

$$\begin{aligned}
l^z_{q\,{}^{1\;14}_{2\;23}} &= \tanh\frac{\beta}{2}\left[\mp(\varepsilon' - \omega') + (\delta_{s6} + \delta_{16})\varepsilon_6 + \frac{1}{\beta}z_{q\,{}^{14}_{23}}\right],\\
n^z_{q\,{}^{1\;14}_{2\;23}} &= \tanh\frac{\beta}{2}\left[\mp(\omega' - \omega'_1) - \delta_{16}\varepsilon_6 + \frac{1}{\beta}z_{q\,{}^{14}_{23}}\right],\\
m^z_{q\,{}^{1\;14}_{4\;23}} &= \tanh\frac{\beta}{2}\left[\mp\omega' - (\pm\delta_{a6} + \delta_{16})\varepsilon_6 + \frac{1}{\beta}z_{q\,{}^{14}_{23}}\right],\\
m^z_{q\,{}^{3\;14}_{2\;23}} &= \tanh\frac{\beta}{2}\left[\mp\omega' - (\mp\delta_{a6} + \delta_{16})\varepsilon_6 + \frac{1}{\beta}z_{q\,{}^{14}_{23}}\right]. \qquad (3.5)
\end{aligned}$$

When an electric field E_3 along the c-axis is applied, the deuteron distribution functions possess the following symmetry

$$\begin{aligned}
&\eta^{(1)z}_{q14} = \langle\sigma_{q1}\rangle = \langle\sigma_{q4}\rangle, && \eta^{(1)z}_{q23} = \langle\sigma_{q2}\rangle = \langle\sigma_{q3}\rangle,\\
&\eta^{(3)z}_{q14} = \langle\sigma_{q2}\sigma_{q3}\sigma_{q4}\rangle = \langle\sigma_{q1}\sigma_{q2}\sigma_{q3}\rangle, && \eta^{(3)z}_{q23} = \langle\sigma_{q1}\sigma_{q3}\sigma_{q4}\rangle = \langle\sigma_{q1}\sigma_{q2}\sigma_{q4}\rangle,\\
&\eta^{(2)z}_{q14} = \langle\sigma_{q1}\sigma_{q4}\rangle, && \eta^{(2)z}_{q23} = \langle\sigma_{q2}\sigma_{q3}\rangle,\\
&\eta^{(2)z}_{q2} = -\langle\sigma_{q1}\sigma_{q2}\rangle = -\langle\sigma_{q3}\sigma_{q4}\rangle, && \eta^{(2)z}_{q3} = -\langle\sigma_{q1}\sigma_{q3}\rangle = -\langle\sigma_{q2}\sigma_{q4}\rangle. \qquad (3.6)
\end{aligned}$$

Substituting (3.3) into the system (3.1) and taking into account the symmetry of the distribution functions (3.6), we obtain the following system of equations for the time-dependent deuteron distribution functions in the presence of the field E_3:

$$\frac{\mathrm{d}}{\mathrm{d}t}\begin{pmatrix}
\eta^{(1)z}_{q14}\\ \eta^{(1)z}_{q23}\\ \eta^{(3)z}_{q14}\\ \eta^{(3)z}_{q23}\\ \eta^{(2)z}_{q14}\\ \eta^{(2)z}_{q23}\\ \eta^{(2)z}_{q2}\\ \eta^{(2)z}_{q3}
\end{pmatrix} = \begin{pmatrix}
\bar{c}_{q11} & \bar{c}_{q12} & \dots & \bar{c}_{q18}\\
\bar{c}_{q21} & \bar{c}_{q22} & \dots & \bar{c}_{q28}\\
\bar{c}_{q31} & \bar{c}_{q32} & \dots & \bar{c}_{q38}\\
\bar{c}_{q41} & \bar{c}_{q42} & \dots & \bar{c}_{q48}\\
\bar{c}_{q51} & \bar{c}_{q52} & \dots & \bar{c}_{q58}\\
\bar{c}_{q61} & \bar{c}_{q62} & \dots & \bar{c}_{q68}\\
\bar{c}_{q71} & \bar{c}_{q72} & \dots & \bar{c}_{q78}\\
\bar{c}_{q81} & \bar{c}_{q82} & \dots & \bar{c}_{q88}
\end{pmatrix}\begin{pmatrix}
\eta^{(1)z}_{q14}\\ \eta^{(1)z}_{q23}\\ \eta^{(3)z}_{q14}\\ \eta^{(3)z}_{q24}\\ \eta^{(2)z}_{q14}\\ \eta^{(2)z}_{q23}\\ \eta^{(2)z}_{q2}\\ \eta^{(2)z}_{q3}
\end{pmatrix} + \begin{pmatrix}
\bar{c}_{q1}\\ \bar{c}_{q2}\\ \bar{c}_{q3}\\ \bar{c}_{q4}\\ \bar{c}_{q5}\\ \bar{c}_{q6}\\ \bar{c}_{q7}\\ \bar{c}_{q8}
\end{pmatrix}. \qquad (3.7)$$

Expressions for the coefficients $\bar{c}_{q11}, \ldots, \bar{c}_{q88}$ are given in [18]. In the one-particle approximation, we obtain the following system of equations

$$\frac{\mathrm{d}}{\mathrm{d}t}\eta_{q14}^{(1)z} = -\frac{1}{\alpha}\eta_{q14}^{(1)z} + \frac{1}{\alpha}\tanh\frac{1}{2}\bar{z}_{q14}\,, \qquad \frac{\mathrm{d}}{\mathrm{d}t}\eta_{q23}^{(1)z} = -\frac{1}{\alpha}\eta_{q23}^{(1)z} + \frac{1}{\alpha}\tanh\frac{1}{2}\bar{z}_{q23}\,. \tag{3.8}$$

We shall consider the vibrations of a thin square plate with sides l of a $ND_4D_2PO_4$ type crystal cut in the [001] plane, produced by an external time-dependent electric field $E_{3\mathrm{t}} = E_3\mathrm{e}^{\mathrm{i}\omega t}$. For the sake of simplicity we shall neglect the diagonal strains ε_i $(i = 1, 2, 3)$, which, in fact, are also created in the crystal.

The shear strain ε_6 is determined by the displacements $u_x = u_1$ and $u_y = u_2$, namely

$$\varepsilon_6 = \varepsilon_{xy} = \frac{\partial u_1}{\partial y} + \frac{\partial u_2}{\partial x}\,.$$

The classical equations of motion of an elementary volume, describing the dynamics of deformational processes in $ND_4D_2PO_4$ type crystals, read

$$\rho\frac{\partial^2 u_1}{\partial t^2} = \frac{\partial\sigma_6}{\partial y}\,, \qquad \rho\frac{\partial^2 u_2}{\partial t^2} = \frac{\partial\sigma_6}{\partial x}\,, \tag{3.9}$$

where ρ is the crystal density.

Taking into account (2.11) and (3.9), we obtain

$$\begin{aligned}
\rho\frac{\partial^2 u_1}{\partial t^2} &= c_{66}^{E0}\frac{\partial\varepsilon_6}{\partial y} + \frac{4\psi_6}{v}\frac{\partial\eta_t^{(1)z}}{\partial y} + \frac{2\delta_{a6}}{v}\frac{\partial}{\partial y}\left(\frac{M_{a6}}{D_6}\right) - \frac{2\delta_{s6}}{v}\frac{\partial}{\partial y}\left(\frac{N_{s6}}{D_6}\right) + \frac{2\delta_{16}}{v}\frac{\partial}{\partial y}\left(\frac{N_{16}\mathrm{ch}x_q}{D_6}\right),\\
\rho\frac{\partial^2 u_2}{\partial t^2} &= c_{66}^{E0}\frac{\partial\varepsilon_6}{\partial x} + \frac{4\psi_6}{v}\frac{\partial\eta_t^{(1)z}}{\partial x} + \frac{2\delta_{a6}}{v}\frac{\partial}{\partial x}\left(\frac{N_{a6}}{D_6}\right) - \frac{2\delta_{s6}}{v}\frac{\partial}{\partial x}\left(\frac{N_{s6}}{D_6}\right) + \frac{2\delta_{16}}{v}\frac{\partial}{\partial x}\left(\frac{N_{16}\mathrm{ch}x_q}{D_6}\right).
\end{aligned} \tag{3.10}$$

Assuming that the crystal is mechanically free, we present the distribution functions, effective fields, and the strain ε_6 as sums of two terms: the equilibrium functions and their fluctuations. Hence

$$\begin{aligned}
\eta_{\substack{q\,14\\ \,23}}^{(1)z} &= \mp\eta_q^{(1)} + \eta_t^{(1)z}, \qquad \eta_{\substack{q\,14\\ \,23}}^{(3)z} = \mp\eta_q^{(3)} + \eta_t^{(3)z},\\
\eta_{q14}^{(2)z} &= \eta_1^{(2)} - \eta_{qt}^{(2)z}, \qquad \eta_{q12}^{(2)z} = \eta_1^{(2)} + \eta_{qt}^{(2)z}, \qquad \eta_{q2}^{(2)z} = -\eta_2^{(2)}, \qquad \eta_{q3}^{(2)z} = -\eta_3^{(2)},\\
\varepsilon_6 &= \varepsilon_{6\mathrm{t}}\,, \qquad E_3 = E_{3\mathrm{t}}\,, \qquad z_{q14} = -x_q + z_t - 2\beta\psi_6\varepsilon_{6\mathrm{t}}\,, \qquad z_{q23} = x_q + z_t - 2\beta\psi_6\varepsilon_{6\mathrm{t}}\,,
\end{aligned} \tag{3.11}$$

where

$$x_q = -\beta\Delta_{qa} + 2\beta\nu_a(\mathbf{k}^z)\eta_q^{(1)}, \qquad z_t = -\beta\Delta_{ct} + 2\beta\nu_c(0)\eta_t^{(1)z} + \beta\mu_3 E_{3\mathrm{t}}\,.$$

The calculated statistical distribution functions in the $ND_4D_2PO_4$ type crystal in the particular case at $E_3 = 0$ and $\sigma_6 = 0$ have the following form

$$\begin{aligned}
\eta^{(1)} &= \frac{1}{D}(\sinh 2x + 2b\sinh x), \quad \eta^{(3)} = \frac{1}{D}(\sinh 2x - 2b\sinh x),\\
\eta_1^{(2)} &= \frac{1}{D}(\cosh 2x - 1 + a + d), \quad \eta_2^{(2)} = \frac{1}{D}(\cosh 2x - 1 - a + d), \quad \eta_3^{(2)} = \frac{1}{D}(\cosh 2x - 1 + a - d).\\
D &= a + \mathrm{ch}2x + d + 4b\mathrm{ch}x + 1, \quad x = \frac{1}{2}\ln\frac{1+\eta^{(1)}}{1-\eta^{(1)}} + \beta\nu_a(\mathbf{k}^z)\eta^{(1)}.
\end{aligned}$$

Let us expand the coefficients (3.4) in series over the time-dependent terms. Taking into account (3.11) and eliminating Δ_{ct} from the system (3.7)–(3.8), we obtain a system of equations for the

time-dependent distribution functions for a mechanically free crystal

$$\frac{\mathrm{d}}{\mathrm{d}t}\begin{pmatrix}\eta_t^{(1)z}\\ \eta_t^{(3)z}\\ \eta_{qt}^{(2)z}\end{pmatrix}=\begin{pmatrix}c_{011}&c_{012}&c_{q13}\\ c_{021}&c_{022}&c_{q23}\\ c_{q31}&c_{q32}&c_{033}\end{pmatrix}\begin{pmatrix}\eta_t^{(1)z}\\ \eta_t^{(3)z}\\ \eta_{qt}^{(2)z}\end{pmatrix}-\frac{\beta\mu_3}{2}E_{3\mathrm{t}}\begin{pmatrix}c_{01}\\ c_{02}\\ c_{q3}\end{pmatrix}$$
$$+\beta\psi_6\varepsilon_{6\mathrm{t}}\begin{pmatrix}c_{01}\\ c_{02}\\ c_{q3}\end{pmatrix}-\beta\delta_{s6}\varepsilon_{6\mathrm{t}}\begin{pmatrix}c_{0s1}\\ c_{0s2}\\ c_{qs3}\end{pmatrix}+\beta\delta_{a6}\varepsilon_{6\mathrm{t}}\begin{pmatrix}c_{0a1}\\ c_{0a2}\\ c_{qa3}\end{pmatrix}-\beta\delta_{16}\varepsilon_{6\mathrm{t}}\begin{pmatrix}c_{061}\\ c_{062}\\ c_{q63}\end{pmatrix}. \quad (3.12)$$

The expressions for coefficients of this system are given in [18].

Taking into account (3.10) and (3.11), we get

$$\rho\frac{\partial^2 u_{1\mathrm{t}}}{\partial t^2}=c_{16}\frac{\partial\varepsilon_{6\mathrm{t}}}{\partial y}+c_{26}\frac{\partial\eta_t^{(1)z}}{\partial y}, \qquad \rho\frac{\partial^2 u_{2\mathrm{t}}}{\partial t^2}=c_{16}\frac{\partial\varepsilon_{6\mathrm{t}}}{\partial x}+c_{26}\frac{\partial\eta_t^{(1)z}}{\partial x}, \quad (3.13)$$

where

$$\begin{aligned}c_{16}&=c_{66}^{E0}+\frac{4\beta\psi_6}{vD}f_6-\frac{2\beta}{vD}\Big[\delta_{s6}^2 a+\delta_{16}^2 4b+\delta_{a6}^2(1+\cosh 2x)\Big],\\ c_{26}&=\frac{4}{v}\left(\psi_6-\frac{\varphi_c^\eta}{D}f_6\right).\\ f_6&=\delta_{s6}a-\delta_{16}2b\mathrm{ch}x, \qquad \varphi_c^\eta=\frac{1}{1-\eta^{(1)2}}+\beta\nu_c(0).\end{aligned} \quad (3.14)$$

We look for the solutions of the systems (3.12) and (3.13) in the form of harmonic waves

$$\begin{aligned}&\eta_t^{(1)z}=\eta_E^{(1)}(x,y)\mathrm{e}^{\mathrm{i}\omega t}, \qquad \eta_t^{(3)z}=\eta_E^{(3)}(x,y)\mathrm{e}^{\mathrm{i}\omega t}, \qquad \eta_t^{(2)z}=\eta_E^{(2)}(x,y)\mathrm{e}^{\mathrm{i}\omega t},\\ &\varepsilon_{6\mathrm{t}}=\varepsilon_{6\mathrm{E}}(x,y)\mathrm{e}^{\mathrm{i}\omega t}, \qquad u_{1\mathrm{t}}=u_{1\mathrm{E}}(y)\mathrm{e}^{\mathrm{i}\omega t}, \quad u_{2\mathrm{t}}=u_{2\mathrm{E}}(x)\mathrm{e}^{\mathrm{i}\omega t}.\end{aligned} \quad (3.15)$$

Solving the system (3.12) with taking into account (3.15), we find that

$$\begin{aligned}\eta_E^{(1)}(x,y) &= \frac{\beta\mu_3}{2}F^{(1)}(\omega)E_3+\Big[-\beta\psi_6F^{(1)}(\omega)-\beta\delta_{s6}F_s^{(1)}(\omega)\\ &\quad-\beta\delta_{a6}F_{a6}^{(1)}(\omega)+\beta\delta_{16}F_1^{(1)}(\omega)\Big]\varepsilon_{6\mathrm{E}}(x,y),\end{aligned} \quad (3.16)$$

where

$$\begin{aligned}F^{(1)}(\omega)&=\frac{(\mathrm{i}\omega)^2r^{(2)}+(\mathrm{i}\omega)r^{(1)}+r^{(0)}}{(\mathrm{i}\omega)^3+(\mathrm{i}\omega)^2r_2+(\mathrm{i}\omega)r_1+r_0}, \quad F_s^{(1)}(\omega)=\frac{(\mathrm{i}\omega)^2r_s^{(2)}+(\mathrm{i}\omega)r_s^{(1)}+r_s^{(0)}}{(\mathrm{i}\omega)^3+(\mathrm{i}\omega)^2r_2+(\mathrm{i}\omega)r_1+r_0},\\ F_a^{(1)}(\omega)&=\frac{(\mathrm{i}\omega)^2r_a^{(2)}+(\mathrm{i}\omega)r_a^{(1)}+r_a^{(0)}}{(\mathrm{i}\omega)^3+(\mathrm{i}\omega)^2r_2+(\mathrm{i}\omega)r_1+r_0}, \quad F_1^{(1)}(\omega)=\frac{(\mathrm{i}\omega)^2r_1^{(2)}+(\mathrm{i}\omega)r_1^{(1)}+r_1^{(0)}}{(\mathrm{i}\omega)^3+(\mathrm{i}\omega)^2r_2+(\mathrm{i}\omega)r_1+r_0},\end{aligned} \quad (3.17)$$

and the expressions for $r_2, \ldots, r_1^{(0)}$ are presented in [18].

Taking into account (3.13) and (3.16), we obtain the following wave equations for $u_{1\mathrm{E}}$ and $u_{2\mathrm{E}}$:

$$\frac{\partial^2 u_{1\mathrm{E}}}{\partial y^2}+k_6u_{1\mathrm{E}}=0, \qquad \frac{\partial^2 u_{2\mathrm{E}}}{\partial x^2}+k_6u_{2\mathrm{E}}=0, \quad (3.18)$$

where the wavenumber is

$$k_6=\frac{\omega\sqrt{\rho}}{\sqrt{c_{66}^E(\omega)}},$$

whereas

$$\begin{aligned}c_{66}^E(\omega) &= c_{66}^{E0}+\frac{4\beta\psi_6}{vD}\Big[-2\psi_6F^{(1)}(\omega)+\delta_{s6}F_s^{(1)}(\omega)+\delta_{16}F_1^{(1)}(\omega)-\delta_{a6}F_a^{(1)}(\omega)\Big]\\ &\quad-\frac{4\varphi_c^\eta f_6}{vD}\beta\Big[-2\psi_6F^{(1)}(\omega)+\delta_{s6}F_s^{(1)}(\omega)+\delta_{16}F_1^{(1)}(\omega)-\delta_{a6}F_a^{(1)}(\omega)\Big]\\ &\quad+\frac{4\beta\psi_6}{vD}f_6-\frac{2\beta}{vD}\Big[\delta_{s6}^2a+\delta_{16}^2 4b+\delta_{a6}^2(1+\cosh 2x)\Big].\end{aligned} \quad (3.19)$$

We look for the solutions of (3.18) in the form

$$u_{1\mathrm{E}} = A_1 \cos k_6 y + B_1 \sin k_6 y, \qquad u_{2\mathrm{E}} = A_2 \cos k_6 x + B_2 \sin k_6 x.$$

As a result,

$$\varepsilon_{6\mathrm{E}}(x,y) = k_6[-(A_1 \cos k_6 y + A_2 \cos k_6 x) + (B_1 \sin k_6 y + B_2 \sin k_6 x)]. \tag{3.20}$$

We set the boundary conditions in the following form

$$\varepsilon_{6\mathrm{E}}(0,0) = \varepsilon_{6\mathrm{E}}(l,l) = \varepsilon_{6\mathrm{E}}(0,l) = \varepsilon_{6\mathrm{E}}(l,0) = \varepsilon_{06}\,. \tag{3.21}$$

Using expressions (2.11) and (3.17), we find that

$$\varepsilon_{06} = \frac{e_{36}(\omega)}{c_{66}^{E}(\omega)} E_3\,, \tag{3.22}$$

where

$$e_{36}(\omega) = e_{36}^{0} + \frac{\beta\mu_3}{v}\Big[-2\psi_6 F^{(1)}(\omega) + \delta_{s6} F_s^{(1)}(\omega) - \delta_{a6} F_a^{(1)}(\omega) + \delta_{16} F_1^{(1)}(\omega)\Big]. \tag{3.23}$$

Taking into account the boundary conditions (3.22) and (3.20), we get

$$\varepsilon_{6\mathrm{E}}(x,y) = \frac{\varepsilon_{06}}{2}\Big[-\frac{\cos k_6 l - 1}{\sin k_6 l}(\sin k_6 y + \sin k_6 x) + (\cos k_6 y + \cos k_6 x)\Big]. \tag{3.24}$$

Using the relation between polarization P_3 and the order parameter $\eta^{(1)}$ and strain ε_6 (2.11), as well as (3.17), we find

$$P_3(x,y,t) = P_{3\mathrm{E}}(x,y)\mathrm{e}^{\mathrm{i}\omega t}, \tag{3.25}$$

where

$$P_{3\mathrm{E}}(x,y) = e_{36}(\omega)\varepsilon_{6\mathrm{E}}(x,y) + \chi_{33}^{\varepsilon}(\omega) E_3\,,$$

and

$$\chi_{33}^{\varepsilon}(\omega) = \chi_{33}^{\varepsilon 0} + \frac{\beta\mu_3^2}{v} F^{(1)}(\omega), \qquad \omega = 2\pi\nu. \tag{3.26}$$

The longitudinal dielectric dynamic permittivity of a $ND_4D_2PO_4$ type crystal can be calculated using the relation

$$\chi_{33}^{\sigma}(\omega) = \frac{1}{l^2}\frac{\partial}{\partial E_3}\int_0^l\int_0^l P_{3\mathrm{E}}(x,y)\mathrm{d}x\mathrm{d}y. \tag{3.27}$$

Since

$$\frac{1}{l^2}\int_0^l\int_0^l \mathrm{d}x\mathrm{d}y\varepsilon_6(x,y) = \frac{2\varepsilon_{06}}{k_6}\tanh\frac{k_6 l}{2} = \frac{\varepsilon_{06}}{R(\omega)}\,, \tag{3.28}$$

where

$$R_6(\omega) = \frac{2}{k_6 l}\tanh\frac{k_6 l}{2},$$

then from (3.27) we find that

$$\chi_{33}^{\sigma}(\omega) = \chi_{33}^{\varepsilon}(\omega) + \frac{1}{R_6(\omega)}\frac{e_{36}^2(\omega)}{c_{66}^{E}(\omega)}\,. \tag{3.29}$$

Thereafter, longitudinal dynamic dielectric permittivity of the $ND_4D_2PO_4$ type crystals is

$$\varepsilon_{33}^{\sigma}(\omega) = 1 + 4\pi\chi_{33}^{\sigma}(\omega). \tag{3.30}$$

It should be noted that at $\omega \to \infty$ $R_6(\omega) \to \infty$ and $\chi_{33}^{\sigma}(\omega) \to \chi_{33}^{\varepsilon}(\omega)$.

4. Sound attenuation and velocity in $ND_4D_2PO_4$ type crystals

We consider propagation through the $ND_4D_2PO_4$ type crystals of a sound wave, whose length is much smaller than sample dimensions. Then, all the dynamic variables, namely, the order parameter and elementary displacements depend only on the spatial coordinate which is the direction of sound propagation. For the thin bars cut along [001] we should consider a transverse ultrasound wave polarized along [010]. Among the derivatives $\frac{\partial u_i}{\partial x_j}$ only $\frac{\partial u_2}{\partial x}$ is different from zero; therefore, instead of (3.12) and (3.13) we can write

$$\frac{\mathrm{d}}{\mathrm{d}t}\begin{pmatrix}\eta_t^{(1)z}\\ \eta_t^{(3)z}\\ \eta_{qt}^{(2)z}\end{pmatrix}=\begin{pmatrix}c_{011}&c_{012}&c_{q13}\\ c_{021}&c_{022}&c_{q23}\\ c_{q31}&c_{q32}&c_{033}\end{pmatrix}\begin{pmatrix}\eta_t^{(1)z}\\ \eta_t^{(3)z}\\ \eta_{qt}^{(2)z}\end{pmatrix}$$
$$+\beta\psi_6\varepsilon_{6\mathrm{t}}\begin{pmatrix}c_{01}\\ c_{02}\\ c_{q3}\end{pmatrix}-\beta\delta_{s6}\varepsilon_{6\mathrm{t}}\begin{pmatrix}c_{0s1}\\ c_{0s2}\\ c_{qs3}\end{pmatrix}+\beta\delta_{a6}\varepsilon_{6\mathrm{t}}\begin{pmatrix}c_{0a1}\\ c_{0a2}\\ c_{qa3}\end{pmatrix}-\beta\delta_{16}\varepsilon_{6\mathrm{t}}\begin{pmatrix}c_{011}\\ c_{012}\\ c_{q13}\end{pmatrix},$$
$$\rho\frac{\partial^2 u_{2\mathrm{t}}}{\partial t^2}=c_{16}\frac{\partial\varepsilon_{6\mathrm{t}}}{\partial x}+c_{26}\frac{\partial\eta_t^{(1)z}}{\partial x}\,. \tag{4.1}$$

Solving the system (4.1), we obtain the wavenumber that coincides with the one found above

$$k_6=\frac{\omega\sqrt{\rho}}{\sqrt{c_{66}^E(\omega)}}\,. \tag{4.2}$$

Using (4.2), we can calculate the ultrasound velocity

$$v_6(\omega)=\frac{\omega}{\mathrm{Re}(k_6)}=\mathrm{Re}\frac{\sqrt{c_{66}^E(\omega)}}{\sqrt{\rho}} \tag{4.3}$$

and attenuation

$$\alpha_6(\omega)=\alpha_{06}-\mathrm{Im}(k_6)=\alpha_{06}-\mathrm{Im}\left(\frac{(\omega)\sqrt{\rho}}{\sqrt{c_{66}^E(\omega)}}\right), \tag{4.4}$$

where α_{06} is the constant frequency and temperature independent term, describing contributions of other mechanisms to the observed attenuation.

5. Longitudinal static dielectric, piezoelectric, and elastic characteristics of $ND_4D_2PO_4$ type crystals

In the static limit $\omega\to 0$ in (3.26), (3.23), and (3.19), we obtain the isothermal static dielectric susceptibility of a mechanically clamped crystal, coefficient of piezoelectric stress, and elastic constant and constant field in the antiferroelectric phase in the following form

$$\chi_{33}^{\varepsilon}=\chi_{33}^{\varepsilon 0}+\frac{\mu_3^2}{v}\beta\frac{2\varkappa_6}{D-2\varkappa_6\varphi_c^{\eta}}\,, \tag{5.1}$$
$$e_{36}=e_{36}^0+2\frac{\mu_3}{v}\beta\frac{-2\varkappa_6+f_6}{D-2\varkappa_6\varphi_c^{\eta}}\,, \tag{5.2}$$
$$c_{66}^E=c_{66}^{E0}+\frac{8\psi_6}{v}\frac{\beta(-\psi_6\varkappa_6+f_6)}{D-2\varkappa_6\varphi_c^{\eta}}-\frac{4\beta\varphi_c^{\eta}f_6^2}{vD(D-2\varkappa_6\varphi_c^{\eta})}-\frac{2\beta}{vD}(\delta_{16}^2 4b\mathrm{ch}x+\delta_{s6}^2 a+\delta_{a6}^2 2\mathrm{ch}^2 x). \tag{5.3}$$

Here we use the notation

$$\varkappa_6=a+b\mathrm{ch}x.$$

In the paraelectric phase, from (5.1)–(5.3) one easily obtains

$$\chi_{33}^{\varepsilon} = \chi_{33}^{\varepsilon 0} + \frac{\mu_3^2}{v}\beta\frac{2(a+b)}{2-a+2b-2\beta\nu_c(0)(a+b)}\,. \tag{5.4}$$

$$e_{36} = e_{36}^{0} + 2\frac{\mu_3}{v}\beta\frac{-2\psi_6(a+b)+\delta_{s6}a-2\delta_{16}b}{-a+2+2b-2\beta\nu_c(0)(a+b)}\,. \tag{5.5}$$

$$\begin{aligned} c_{66}^{E} = {} & c_{66}^{E0} + \frac{8\psi_6}{v}\beta\frac{-2\psi_6(a+b)+\delta_{s6}a-2\delta_{16}b}{-a+2+2b-2\beta\nu_c(0)(a+b)} \\ & - \frac{4\beta}{v}\frac{[1+\beta\nu_c(0)](\delta_{s6}a-2\delta_{16}b)^2}{(2+a+4b)[-a+2+2b-2\beta\nu_c(0)(a+b)]} - \frac{2\beta}{v}\frac{\delta_{s6}^2 a+\delta_{16}^2 4b+2\delta_{a6}^2}{2+a+4b}\,. \end{aligned} \tag{5.6}$$

Using the known relations between elastic, dielectric, and piezoelectric characteristics, we find the isothermal constant of piezoelectric stress h_{36}:

$$h_{36} = \frac{e_{36}}{\chi_{33}^{\varepsilon}}; \tag{5.7}$$

isothermal elastic constant at constant polarization c_{66}^{P}:

$$c_{66}^{P} = c_{66}^{E} + e_{36}h_{36}; \tag{5.8}$$

isothermal coefficient of piezoelectric strain d_{36}:

$$d_{36} = \frac{e_{36}}{c_{66}^{E}}; \tag{5.9}$$

isothermal constant of piezoelectric strain g_{36}:

$$g_{36} = \frac{h_{36}}{c_{66}^{P}}; \tag{5.10}$$

isothermal dielectric susceptibility at $\sigma = \text{const}$:

$$\chi_{33}^{\sigma} = \chi_{33}^{\varepsilon} + e_{36}d_{36}\,. \tag{5.11}$$

6. Comparison of numerical calculations with experimental data

Let us now evaluate the found above longitudinal dielectric, piezoelectric, and elastic characteristics of the $NH_4H_2PO_4$ (ADP) and $ND_4D_2PO_4$ (DADP) crystals and compare them with the corresponding experimental data. It should be noted that the developed theory is valid, strictly speaking, only for highly deuterated $ND_4D_2PO_4$ type crystals. The experimentally established relaxational character of $\varepsilon_{33}^{*}(\omega, T)$ dispersion [27–29] in these crystals, according to [13–15] is most likely related to suppression of tunneling by the short-range interactions. Therefore, proton tunneling for the $NH_4H_2PO_4$ type crystals will be neglected. Since the majority of experimental studies were performed for the paraelectric phase, we shall also restrict our calculations to temperatures $T > T_{\mathrm{N}}$.

To calculate the paraelectric temperature and frequency dependences of the physical characteristics of the $NH_4H_2PO_4$ and $ND_4D_2PO_4$ crystals we need to set the values of the following parameters:

– energies of proton and deuteron configurations $\varepsilon'_{\mathrm{H}}$, w'_{H}, $w'_{1\mathrm{H}}$, $\varepsilon'_{\mathrm{D}}$, w'_{D}, $w'_{1\mathrm{D}}$;
– the long–range interaction parameters $\nu_{c\mathrm{H}}(0)$ and $\nu_{c\mathrm{D}}(0)$;
– deformational potentials ψ_6, δ_{s6}, δ_{16}, δ_{a6}, $\delta_{1\mathrm{i}}$;
– effective dipole moments $\mu_{3\mathrm{H}}$ and $\mu_{3\mathrm{D}}$;
– "seed" static dielectric susceptibility $\chi_{33}^{\varepsilon 0}$, coefficient of piezoelectric stress e_{36}^{0}, elastic constants c_{66}^{E0}, c_{ij}^{E0};
– parameters α_{H}, α_{D}.

The volumes of the primitive cell v were taken to be equal to $0{,}2110{\cdot}10^{-21}$ cm^3 for $NH_4H_2PO_4$ [30], and $0{,}213{\cdot}10^{-21}$ cm^3 for $ND_4D_2PO_4$ [31]; whereas the crystal density is $\rho = 1,804$ g/cm^3 [32] both for $NH_4H_2PO_4$ and $ND_4D_2PO_4$.

To determine the mentioned parameters we use the experimental temperature dependences of the physical characteristics of ADP and DADP crystals. Thus, for ADP we used the data for $\varepsilon^{\sigma}_{33}(0,T)$ [32,33], $\varepsilon^{*}_{33}(\omega,T)$ [29], $d_{36}(T)$ [32], $s^{E,P}_{66}(T)$ [32], $s^{E}_{ij}(T)$ [32], whereas for DADP we use $\varepsilon^{\sigma}_{33}(0,T)$ [34], $\varepsilon^{*}_{33}(\omega,T)$ [29], $d_{36}(T)$ [34], $s^{E}_{66}(T)$ [34], s^{E}_{ij} [34]. Also, using the known relations for dielectric, piezoelectric, and elastic characteristics of ADP and DADP, we calculated, using the experimental data of [32,34], the "experimental" temperature dependences of $c^{E}_{66} = \frac{1}{s^{E}_{66}}$, $e_{36} = \frac{d_{36}}{s^{E}_{66}}$, $\varepsilon^{\varepsilon}_{33} = \varepsilon^{\sigma}_{33} - 4\pi\frac{d^2_{36}}{s^{E}_{66}}$, $h_{36} = \frac{d_{36}}{\chi^{\sigma}_{33}s^{E}_{66} - d^2_{36}}$, $c^{P}_{66} = c^{E}_{66} + e_{36}h_{36}$, $g_{36} = \frac{h_{36}}{c^{P}_{66}}$.

Using the experimental data for $\varepsilon^{\sigma}_{33}(0,T)$–$\varepsilon^{0\sigma}_{33}$, $\varepsilon^{'\varepsilon}_{33}(\omega,T)$–$\varepsilon^{0\varepsilon}_{33}$ and $T_{\rm N}$, we determined the parameters ε', w', $\nu_c(0)$, at which the value μ_3 is weakly temperature dependent. Then, using the experimental data for $\varepsilon^{*}_{33}(\omega,T)$, we determine the value of α, which turns out to be also weakly temperature dependent: $\alpha = [P + R(\Delta T)] \cdot 10^{-14}$ ($\Delta T = T - T_{\rm N}$). The energy w'_1 of the proton configurations without any proton and with four protons next to the PO_4 group is much larger than ε' or w'. Hereafter we take $w'_1 = \infty$ ($d = 0$).

The "seed" quantities $\chi^{\varepsilon 0}_{33}$, e^{0}_{36}, $c^{E0}_{66} = \frac{1}{s^{E0}_{66}}$ are determined by fitting the theoretical curves of the characteristics to the experimental points at temperatures far from the transition point $T_{\rm N}$.

To determine the deformational parameters ψ_6, δ_{s6}, δ_{a6}, δ_{16} we explore their effect on the temperature curves of the calculated piezoelectric characteristics d_{36}, e_{36}, h_{36}, g_{36} and of the elastic constant c^{E}_{66} and find such a set of the parameters, yielding a good agreement with experimental data [32,34].

The obtained optimum set of the model parameters for ADP and DADP is given in table 1.

Table 1. Optimum sets of the model parameters for ADP and DADP crystals.

	$T_{\rm N}$, (K)	$\frac{\varepsilon'}{k_{\rm B}}$, (K)	$\frac{w'}{k_{\rm B}}$, (K)	$\frac{\nu_c(0)}{k_{\rm B}}$, (K)	$\mu_3, 10^{-18}$, (esu· cm)	$\chi^{0\varepsilon}_{33}$	P, (s)	R, (s/k)
ADP	148	20	490,0	-10,00	2,10	0,23	0,38	0,0090
DADP	240	78,8	715,4	-17,35	2,75	0,34	6,72	0,0090

	$\frac{\psi_6}{k_{\rm B}}$, (K)	$\frac{\delta_{s6}}{k_{\rm B}}$, (K)	$\frac{\delta_{a6}}{k_{\rm B}}$, (K)	$\frac{\delta_{16}}{k_{\rm B}}$, (K)	$c^{0}_{66} \cdot 10^{-10}$ (dyn/cm^2)	e^{0}_{36} (esu/cm^2)
ADP	-160	1400	100	-300	7.9	10000
DADP	-200	2000	200	-100	7.6	28000

Let us note that using the relations $\varepsilon = -\varepsilon'$ and $w = w' - \varepsilon$, we obtain practically the same values of the proton and deuteron configuration energies of ADP and DADP crystals, as in [21]. In figures 1a and 1b we show the temperature curves of the calculated longitudinal static dielectric permittivities of mechanically free and clamped ADP and DADP crystals along with the available experimental data. Hereafter, in figures for the ADP crystal the dashed lines denote the theoretical temperature curves calculated within the theory that takes tunneling into account [6]. As one can see in figure 1, a satisfactory quantitative description of the experimental data is obtained. The static dielectric permittivities of free and clamped ADP and DADP crystals have finite values at the transition points and are weakly decreasing functions of temperature. The permittivity $\varepsilon^{\sigma}_{33}$ of a free crystal is about $\sim 18\%$ larger than the permittivity $\varepsilon^{\varepsilon}_{33}$ of a clamped crystal; this difference is practically temperature independent. Let us note (see [16]) that in the case of KH_2PO_4 the values of $\varepsilon^{\sigma}_{33}(0)$ increase by the hyperbolic law at approaching $T_{\rm c}$ in the paraelectric phase and are very large at $T = T_{\rm c}$. The difference between $\varepsilon^{\sigma}_{33}(0)$ and $\varepsilon^{\varepsilon}_{33}(0)$ rapidly decreases with temperature increasing.

The calculated temperature dependences of the coefficients of piezoelectric strain d_{36} and stress e_{36} of ADP and DADP crystals along with the experimental points are given in figures 2, 3. A

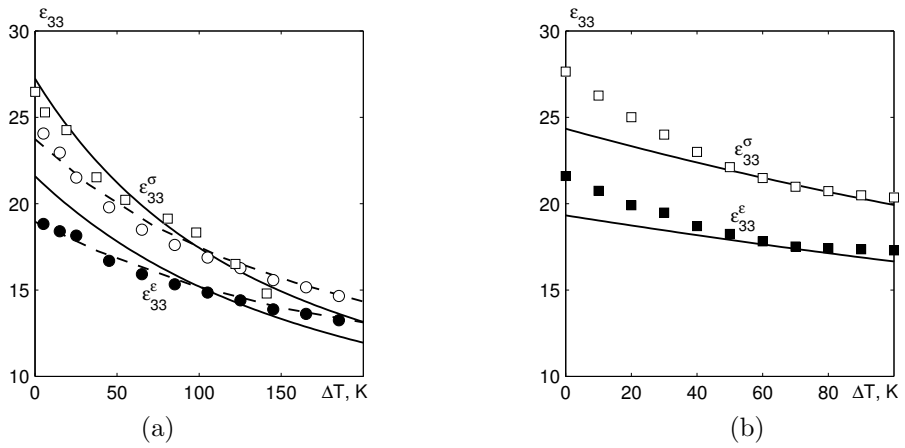

Figure 1. The temperature dependence of static dielectric permittivities of a clamped $\varepsilon_{33}^{\varepsilon}$ •, [32] and free $\varepsilon_{33}^{\sigma}$ ∘ [32], □ [33] $NH_4H_2PO_4$ crystal (a), as well as clamped ■, [34] and free □, [34] $N(H_{0.02}D_{0.98})_4(H_{0.02}D_{0.98})_2PO_4$ crystal (b).

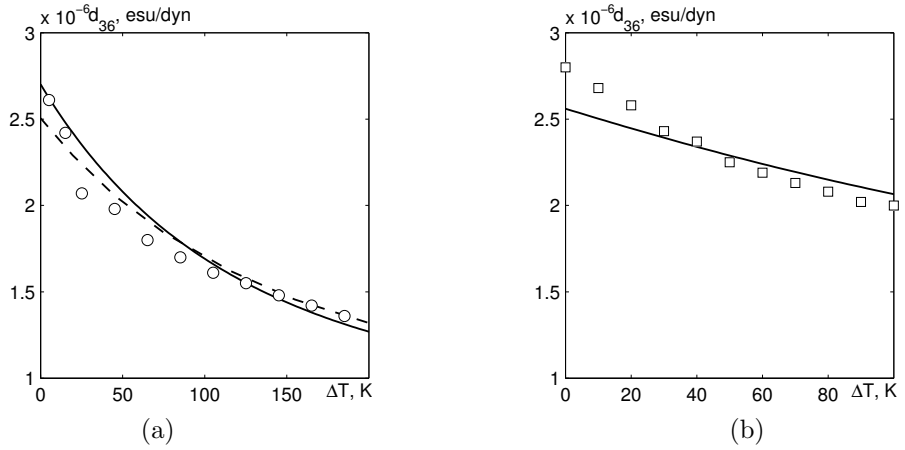

Figure 2. The temperature dependence of the coefficient of piezoelectric strain d_{36} of $NH_4H_2PO_4$ ∘, [32]; $N(H_{0.02}D_{0.98})_4(H_{0.02}D_{0.98})_2PO_4$ □, [34].

good quantitative description of the experimental points is obtained. At $T = T_N$ the coefficients d_{36} and e_{36} are finite and decrease with temperature increasing. The coefficients d_{36} and e_{36} of KH_2PO_4 at $T = T_c$ are about one order of magnitude larger than the corresponding values in the ADP crystal and decrease with temperature increasing much faster than the coefficients d_{36} and e_{36} of ADP [16].

In figures 4 and 5 we plot the temperature dependences of the constants of piezoelectric stress h_{36} and piezoelectric strain g_{36} of ADP and DADP crystals. The experimental data are well described by the proposed theory. The constants h_{36} and g_{36} are practically temperature independent. The temperature dependences of the h_{36} and g_{36} constants of KH_2PO_4 are also weak, with their values being nearly three times smaller than the values of h_{36} and g_{36} of ADP. Even though the dielectric permittivities of ADP and DADP along the c-axis are relatively small, the values of the constants of piezoelectric strain and piezoelectric stress in this direction are rather significant.

The temperature dependences of the calculated isothermal elastic constants c_{66}^E and c_{66}^P of ADP (a) and DADP (b) well agree with the corresponding experimental data (see figure 6). The elastic constants c_{66}^E of ADP and DADP, in contrast to those of KH_2PO_4, are finite at $T = T_N$ and hardly depend on temperature.

Let us analyse now the temperature and frequency dependences of the calculated dynamic

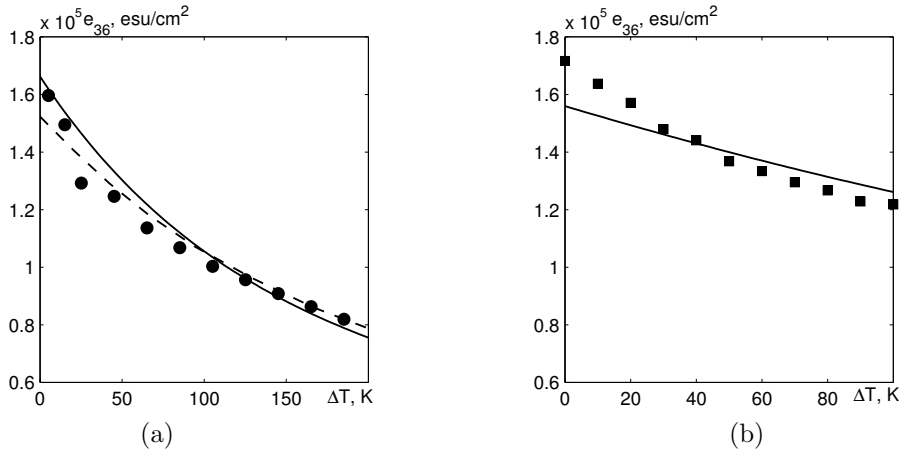

Figure 3. The temperature dependence of the coefficient of piezoelectric stress e_{36} of $NH_4H_2PO_4$ •, [32]; $N(H_{0.02}D_{0.98})_4(H_{0.02}D_{0.98})_2PO_4$ ■, [34].

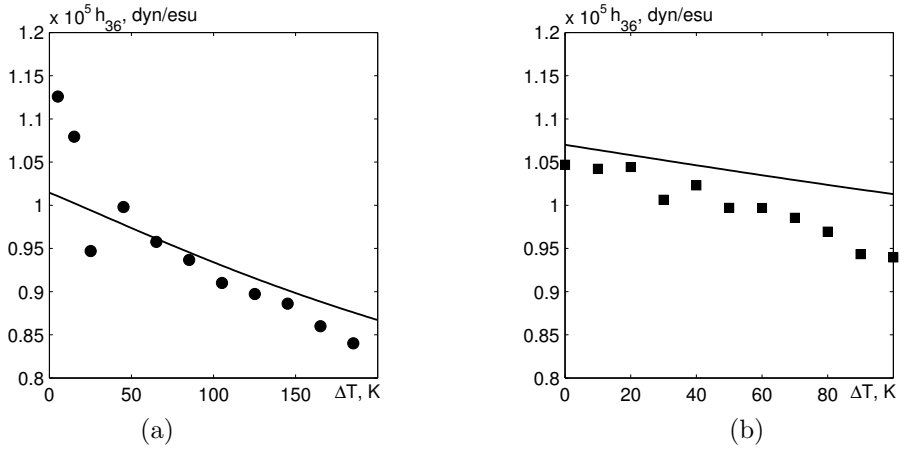

Figure 4. The temperature dependences of the constant of piezoelectric stress h_{36} of $NH_4H_2PO_4$ •, [32]; $N(H_{0.02}D_{0.98})_4(H_{0.02}D_{0.98})_2PO_4$ ■, [34].

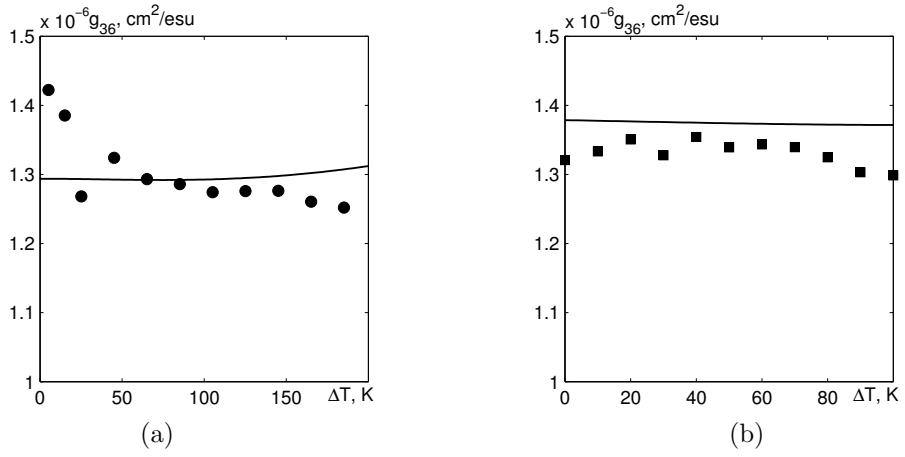

Figure 5. The temperature dependences of the constant of piezoelectric strain g_{36} of $NH_4H_2PO_4$ •, [32]; $N(H_{0.02}D_{0.98})_4(H_{0.02}D_{0.98})_2PO_4$ ■, [34].

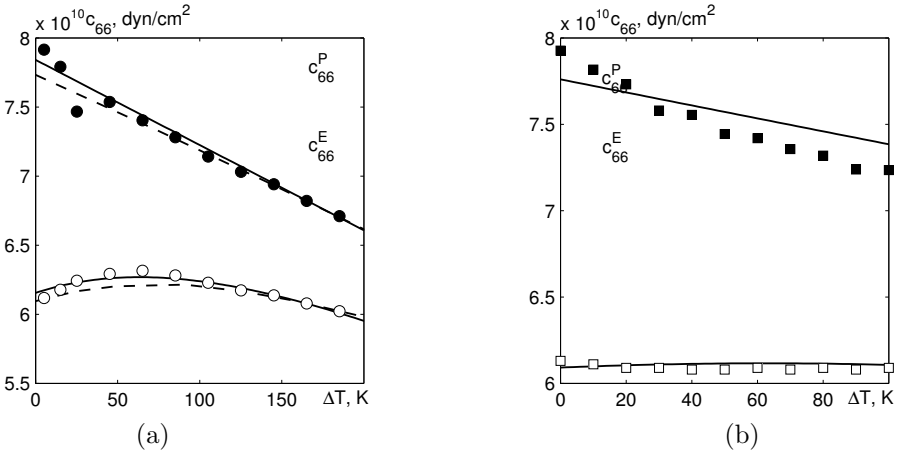

Figure 6. The temperature dependences of the elastic constants c_{66}^E •, [32] and c_{66}^P ∘ [32] of $NH_4H_2PO_4$; c_{66}^E ■, [34] and c_{66}^P □, [34] of $N(H_{0.02}D_{0.98})_4(H_{0.02}D_{0.98})_2PO_4$.

characteristics of mechanically free ADP and DADP crystals cut in the [001] plane as thin square plates with sides $l = 1$ mm long. Unfortunately, we are not aware of a corresponding experimental measurement. From the equation for resonance frequencies

$$\nu_n = \frac{2n+1}{2l}\sqrt{\frac{c_{66}^E}{\rho}}$$

for $NH_4H_2PO_4$ and $n = 1$ we obtain the value of the first resonance frequency $\nu_1 \approx 0.92793$ MHz at $\Delta T = 28$ K. Depending on frequency ν (in the resonance region) and temperature ΔT, the temperature curves of real and imaginary parts of dielectric permittivity of mechanically free ADP and DADP crystals exhibit one, two, or more resonance peaks.

The calculated frequency curves of real and imaginary parts of dielectric permittivity $\varepsilon_{33}^*(\omega, T)$ and experimental points of [29] are presented in figure 7 for ADP at $\Delta T = 28$ K and in figure 8 for DADP at $\Delta T = 64$ K. In the frequency range of $10^6 - 10^8$ Hz a resonance dispersion is observed.

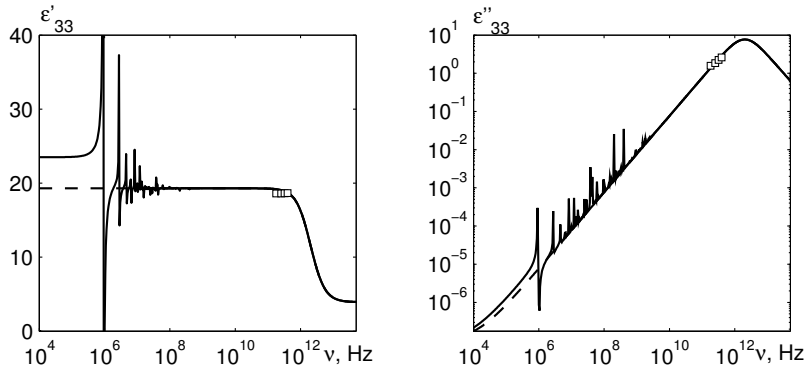

Figure 7. Frequency curves of real and imaginary part of dielectric permittivity of free and clamped (dashed line) $NH_4H_2PO_4$ crystals at $\Delta T = 28$ K, □ – [29].

At $\omega \to 0$ we obtain a static dielectric permittivity of a free crystal. The dashed line corresponds to the low-frequency part of the clamped permittivity. Above the resonances, the permittivity corresponds to a clamped crystal and has a relaxational character.

Theoretical results and experimental points for the temperature dependences of real and imaginary parts of complex dielectric permittivity $\varepsilon_{33}^*(\omega, T)$ of ADP and DADP at frequencies where

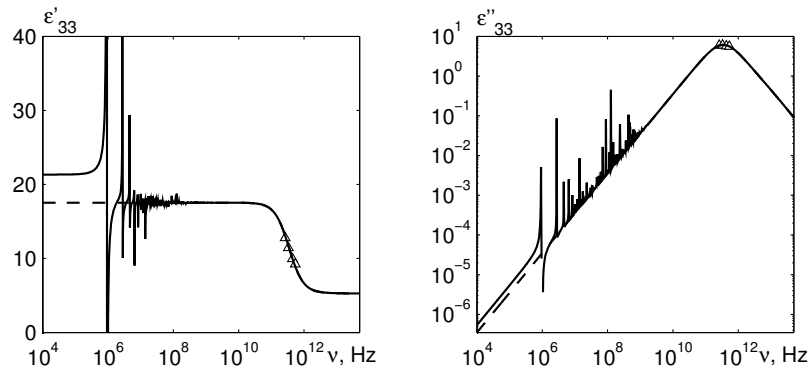

Figure 8. Frequency curves of real and imaginary part of dielectric permittivity of free and clamped (dashed line) $N(H_{0.02}D_{0.98})_4(H_{0.02}D_{0.98})_2PO_4$ crystals at $\Delta T = 64$ K, △ – [27,29].

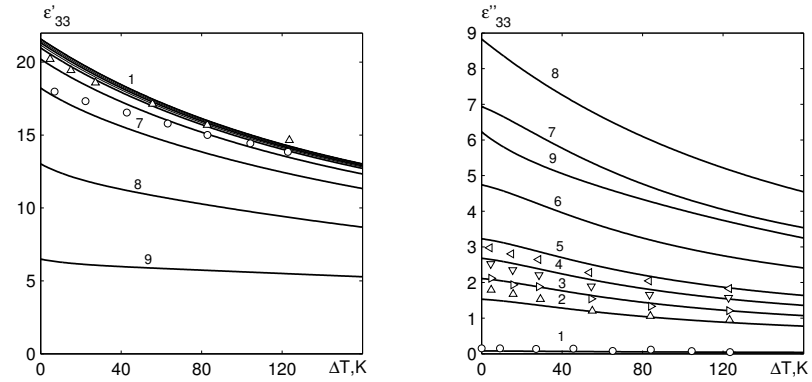

Figure 9. The temperature dependence of ε'_{33} and ε''_{33} of $NH_4H_2PO_4$ at different frequencies ν (GHz): 9.2 – 1, ○[35]; 180.0 – 2, △[29]; 249.9 – 3, ▷[29]; 320.1 – 4, ▽[29]; 390.0 – 5, ◁[29]; 600.0 – 6; 1000.0 – 7; 2000.0 – 8; 5000.0 – 9. Symbols are experimental points; lines are theoretical results.

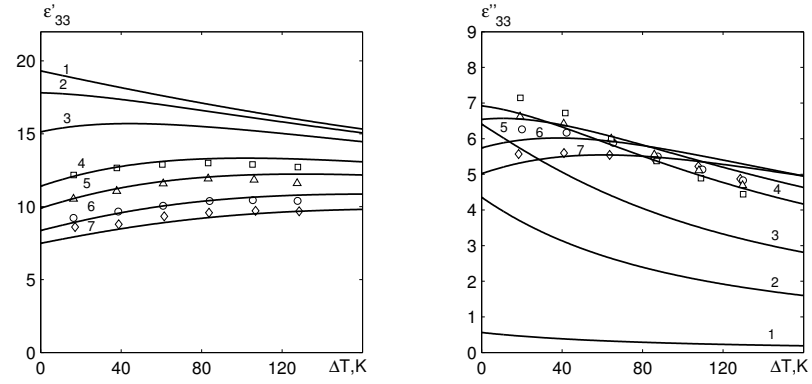

Figure 10. The temperature dependence of ε'_{33} and ε''_{33} of $N(H_{0.02}D_{0.98})_4(H_{0.02}D_{0.98})_2PO_4$ at different frequencies ν (GHz): 9.2 – 1; 80.0 – 2; 150.0 – 3; 262.0 – 4, □[27,29]; 330.0 – 5 △[27,29]; 437.0 – 6 ○[27,29]; 540.0 – 7 ◊[27,29]. Symbols are experimental points; lines are theoretical results.

the effect of crystal clamping by a high-frequency field takes place are given in figures 9, 10, respectively. As one can see, the experimental data of [27,29] are quantitatively well described by the proposed theory. At the transition temperature the real and imaginary parts of permittivity $\varepsilon^*_{33}(\omega, T)$ of ADP have finite maxima at all frequencies. With ΔT increasing the values of $\varepsilon'_{33}(\omega, T)$ and $\varepsilon''_{33}(\omega, T)$ slightly decrease at all frequencies.

In the temperature curves of $\varepsilon'_{33}(\omega, T)$ and $\varepsilon''_{33}(\omega, T)$ of DADP a maximum is observed at $T = T_N$ at frequencies below the dispersion frequency and there is a shallow minimum at higher frequencies. With ΔT increasing at dispersion frequencies the values of $\varepsilon'_{33}(\omega, T)$ and $\varepsilon''_{33}(\omega, T)$ increase, reaching a maximum, which shifts to higher ΔT with frequency increasing.

The calculated frequency dependences of $\varepsilon^*_{33}(\omega, T)$ along with the experimental points are presented in figure 11 for ADP and in figure 12 for DADP. A good quantitative description of

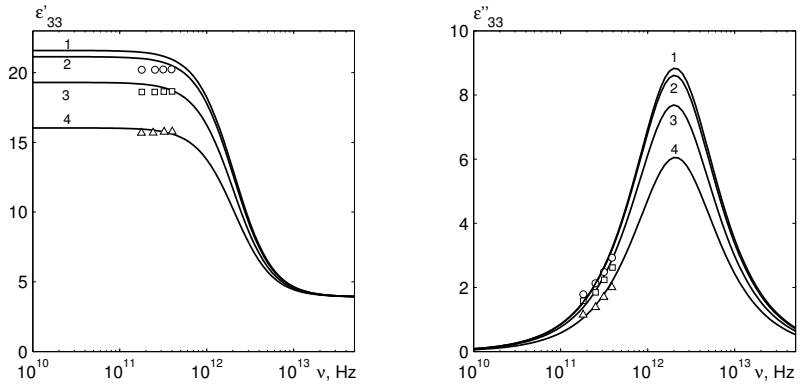

Figure 11. Frequency dependence of ε'_{33} and ε''_{33} of $NH_4H_2PO_4$ at different temperatures ΔT(K) [29]: 0.0 – 1; 5.0 – 2, ○; 28.0 – 3, □; 82.0 – 4, △. Symbols are experimental points; lines are theoretical results.

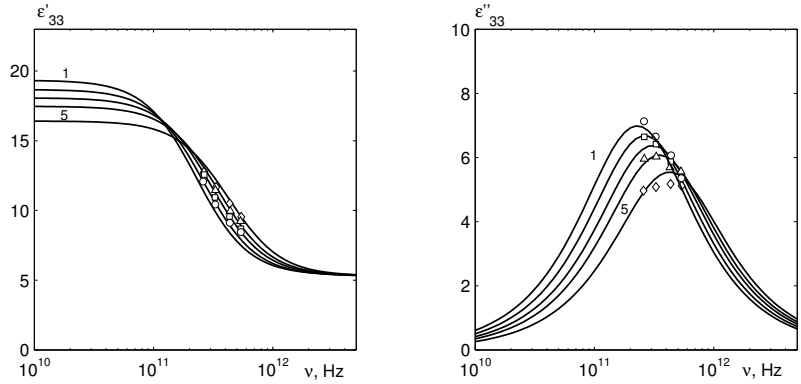

Figure 12. Frequency dependence of ε'_{33} and ε''_{33} of the $N(H_{0.02}D_{0.98})_4(H_{0.02}D_{0.98})_2PO_4$ crystal at different temperatures ΔT(K) [27,29]: 0.0 – 1; 19.0 – 2, ○; 41.0 – 3, □; 64.0 – 4, △; 108.0 – 5, ◇. Symbols are experimental points; lines are theoretical results.

experimental data is obtained. The experimental frequency dependences of $\varepsilon^*_{33}(\omega, T)$ for DADP are for the dispersion region $(10^{11} - -10^{13} Hz)$, whereas for ADP they are below the dispersion. At $\Delta T = 0$ K the dispersion frequency for ADP equals 2062 GHz, whereas for DADP it is 228.5 GHz. With temperature ΔT increasing the dispersion frequency of $\varepsilon^*_{33}(\omega, T)$ slightly increases in DADP and does not change in ADP.

The temperature and frequency dependences of sound attenuation α_6 of ADP and DADP

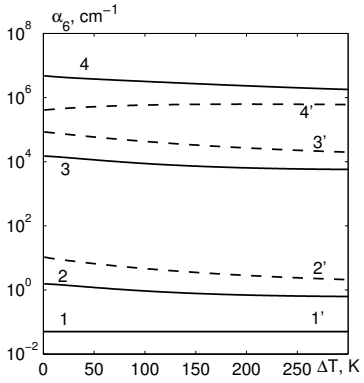

Figure 13. Temperature dependence of sound attenuation α_6 of $NH_4H_2PO_4$ (1,2,3,4), $N(H_{0.02}D_{0.98})_4(H_{0.02}D_{0.98})_2PO_4$ (1',2',3',4') crystals at different frequencies ν, Hz: 1,1' – 10^6, 2,2' – 10^9, 3,3' – 10^{11}, 4,4' – 10^{13}, and DADP at the same frequencies.

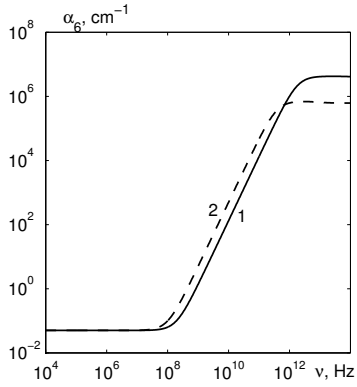

Figure 14. Frequency dependence of sound attenuation α_6 of $NH_4H_2PO_4$ (1) and $N(H_{0.02}D_{0.98})_4(H_{0.02}D_{0.98})_2PO_4$ (2) crystals at ΔT=28K and 64K, respectively.

crystals are shown in figure 13, 14, respectively. At $T = T_N$ the attenuation α_6 is finite and slightly decreases with temperature increasing. Below 10^8 Hz attenuation α_6 is small, whereas at further increase of frequency up to 10^{11} Hz α_6 it rapidly increases and saturates. Such high values of α_6 at saturation mean that sound does not propagate in the crystal. In contrast, in the KH_2PO_4 type crystals, the attenuation rapidly increases at temperatures close to $T = T_c$.

In figure 15 we plot the calculated temperature dependence of the sound velocity v_6 for ADP(a) and DADP(b) crystals. The sound velocity is practically independent of temperature and frequency,

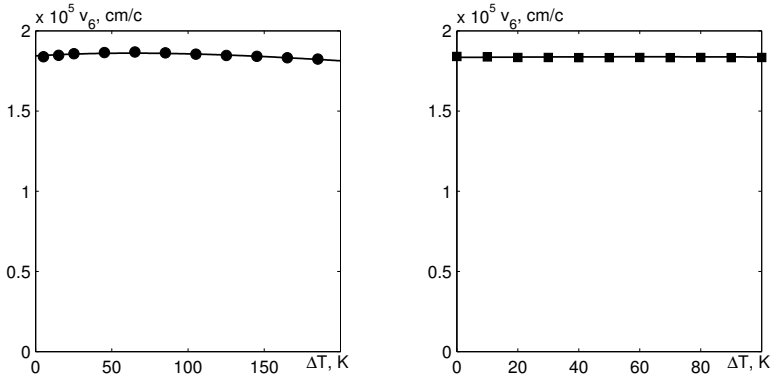

Figure 15. The temperature dependence of sound velocity in the $NH_4H_2PO_4$ (a) and $N(H_{0.02}D_{0.98})_4(H_{0.02}D_{0.98})_2PO_4$ (b) crystals. •, ■ are calculated as $v_6 = \frac{\sqrt{c^E_{44}}}{\sqrt{\rho}}$ [32,34].

except for the frequency region where the dispersion of the clamped dielectric permittivity is observed; in this region the sound velocity v_{66} rapidly increases and saturates.

7. Concluding remarks

In this paper, using the modified proton ordering model for the KH_2PO_4 family crystals, with taking into account the linear in the strain ε_6 contribution to the proton system energy, without

tunneling, within the framework of the four-particle cluster approximation, we develop a theory of dynamic longitudinal dielectric, piezoelectric, and elastic properties of the $ND_4D_2PO_4$ type antiferroelectrics. Sound velocity and attenuation in these crystals are also calculated. Numerical analysis of the dependences of the found characteristics on the values of the theory parameters is performed. Optimum sets of the model parameters and "seed" quantities for $ND_4D_2PO_4$ and $NH_4H_2PO_4$ crystals are found. They permit a satisfactory description of the available experimental data.

The piezoelectric coupling ($\psi_6 \neq 0$) being taken into account gave rise to understandable differences between static dielectric permittivities of mechanically free $\varepsilon_{33}^{\sigma}$ and clamped $\varepsilon_{33}^{\varepsilon}$ crystals. In the ADP type crystals, the permittivity $\varepsilon_{33}^{\sigma}$ is $\approx 18\%$ larger than $\varepsilon_{33}^{\varepsilon}$, and this difference is practically temperature independent. The isothermal elastic constants c_{66}^{P} and c_{66}^{E} in ADP and DADP crystals are different, just like in the KH_2PO_4 type crystals, but they have no peculiarities at $T = T_{\mathrm{N}}$. The sound attenuation coefficient α_6 in the ADP type antiferroelectrics is finite and has a weak temperature dependence, whereas in the KDP type ferroelectrics it has an anomalous behavior in the phase transition region.

The obtained results for the ADP crystals are compared with the calculations performed in [6,7]. It is established that tunneling practically does not affect the static dielectric, piezoelectric, and elastic characteristics of ADP.

References

1. Yomosa Sh., Nagamiya T., Progr. Theor. Phys., 1949, **4**, No. 3, 263.
2. Slater J.C., J. Chem. Phys., 1941, **9**, No. 1, 16.
3. Stasyuk I.V., Biletskii I.N., Izv. AN SSSR, ser. fiz., 1983, **47**, 705 (in Russian).
4. Stasyuk I.V., Biletskii I.N., Styagar O.N., Ukr. J. Phys., 1986, **31**, No. 4, 567.
5. Stasyuk I.V., Levitskii R.R., Zachek I.R., Moina A.P., Phys. Rev. B, 2000, **62**, No. 10, 6198.
6. Levitskii R.R., Lisnii B.M., J. phys. study, 2003, **7**, No. 4, 431 (in Ukrainian).
7. Levitskii R.R., Lisnii B.M., phys. stat. sol. (b), 2004, **241**, No. 6, 1350.
8. Lisnii B.M., Levitskii R.R., Ukr. J. Phys., 2004, **49**, No. 7, 701.
9. Stasyuk I.V., Levitskii R.R., Moina A.P., Lisnii B.M., Ferroelectrics, 2001, **254**, 213.
10. Lisnii B.M., Levitskii R.R., Baran O.R., Phase Transitions, 2007, **80**, No. 1-2, 25.
11. Stasyuk I.V., Levitskii R.R., Moina A.P., Velychko O.V., Ukr. J. Phys.: Reviews, 2008, No. 1, 3 (in Ukrainian).
12. Stasyuk I.V., Kaminska N.M., Ukr. J. Phys., 1974, **19**, No. 2, 237 (in Ukrainian).
13. Stasyuk I.V., Levitskii R.R., Korinevskii N.A., Phys. Stat. Sol. (b), 1979, **91**, No. 2, 541.
14. Levitskii R.R., Stasyuk I.V., Korinevsky H.A., Ferroelectrics, 1978, **21**, 481.
15. Korinevskii N.A., Levitskii R.R., Teor. Mat. Fiz., 1980, **42**, No. 3, 416 (in Russian).
16. Levitskii R.R., Zachek I.R., Vdovych A.S. Preprint of the Institute for Condensed Matter Physics, ICMP-06-08U, Lviv, 2006 (in Ukrainian).
17. Levitskii R.R., Zachek I.R., Vdovych A.S. Preprint of the Institute for Condensed Matter Physics, ICMP-07-24U, Lviv, 2007 (in Ukrainian).
18. Levitskii R.R., Zachek I.R., Vdovych A.S. Preprint of the Institute for Condensed Matter Physics, ICMP-08-19U, Lviv, 2008 (in Ukrainian).
19. Levitskii R.R., Zachek I.R., Vdovych A.S. Preprint of the Institute for Condensed Matter Physics, ICMP-08-20U, Lviv, 2008 (in Ukrainian).
20. Levitsky R.R., Zachek I.R., Mits Ye.V., Moina A.P. Physical collection. Lviv: NTS, 1998, **3**, 417 (in Ukrainian).
21. Levitsky R.R., Zachek I.R., Vdovych A.S., Sorokov S.I. Condens. Matter Phys., 2009, **12**, No. 1, 603.
22. Levitsky R.R., Vdovych A.S., Zachek I.R., Visnyk NULP, fiz. mat. nauky, 2008, **601**, No. 625, 65 (in Ukrainian).
23. Moina A.P. Levitskii R.R., Zachek I.R., Phys. Rev. B, 2005, **71**, 134108.
24. Levitsky R.R., Zachek I.R., Moina A.P., Vdovych A.S., Condens. Matter Phys., 2008, **11**, No. 3(55), 555.
25. Levitskii R.R., Korinevskii N.A., Stasyuk I.V., Ukr. J. Phys., 1974, **19**, No. 8, 1289 (in Russian).
26. Glauber J., J. Math. Phys., 1963, **4**, No. 2, 294.

27. Levitsky R.R., Zachek I.R., Mits Ye.V., Volkov. A.A., Kozlov G.V., Lebedev S.P., Preprint of the Bogolyubov Institute for Theoretical Physics, ITP-82-2R, Kyiv, 1982 (in Russian).
28. Volkov A.A., Kozlov G.V., Lebedev S.P., Fiz. Tverd. Tela, 1980, **22**, No. 10, 3064 (in Russian).
29. Kozlov G.V., Lebedev S.P., Prokhorov A.M., Volkov A.A., J. Phys. Soc. Japan, 1980, **49**, 188.
30. Fukami T., J. Phys. Soc. Jpn., 1988, **57**, No. 4, 1287.
31. Kentsig V. Ferroelectrics and antiferroelectrics, Moscow, 1960 (in Russian).
32. Mason W. Piezoelectric crystals and their application in ultraacoustics, Moscow, 1952 (in Russian).
33. Matthias B., Merz W., Scherrer P., Helv. Phys. Acta, 1947, **20**, 273.
34. Mason W.P., Mattias B.T., Phys. Rev., 1952, **88**, No. 3, 477.
35. Kaminov I.P., Phys. Rev., 1965, **138**, No. 5A, 1539.

Поздовжня релаксація антисегнетоелектриків типу $ND_4D_2PO_4$. П'єзоелектричний резонанс та поглинання звуку

Р.Р.Левицький[1], І.Р.Зачек[2], А.Р.Моїна[1], А.С.Вдович[1]

[1] Інститут фізики конденсованих систем НАН України, 79011 Львів, вул. Свєнціцького, 1, Україна
[2] Національний університет "Львівська політехніка", 79013 Львів, вул. С. Бандери, 12, Україна

Отримано 2 квітня 2009 р., в остаточному вигляді – 18 травня 2009 р.

В рамках модифікованої протонної моделі з врахуванням взаємодії зі зсувною деформацією ε_6 розглянуто динамічний діелектричний відгук антисегнетоелектриків типу $ND_4D_2PO_4$. Враховано динаміку п'єзоелектричної деформації. Явно описано явища затискання кристалу високочастотним електричним полем, п'єзоелектричного резонансу і НВЧ дисперсії, що спостерігаються на експерименті. Розраховано швидкість та коефіцієнт поглинання звуку. Передбачено характер поведінки коефіцієнта поглинання в парафазі та наявність обрізаючої частоти у частотній залежності коефіцієнта поглинання звуку. При належному виборі мікропараметрів в параелектричній фазі отримано добрий кількісний опис експериментальних даних для поздовжніх статичних діелектричних, п'єзоелектричних і пружних характеристик та швидкості звуку для $ND_4D_2PO_4$ і $NH_4H_2PO_4$.

Ключові слова: *антисегнетоелектрики, діелектрична проникність, п'єзоелектричний резонанс*

PACS: *77.22.Ch, 77.22.Gm, 77.65.Bn 77.84.Fa, 77.65.Fs*